Renner-Teller effects in the photoelectron spectra of CNC, CCN, and HCCN

Laurent Coudert, Bérenger Gans, Gustavo Garcia, Jean-Christophe Loison

Renner-Teller effects in the photoelectron spectra of CNC, CCN, and HCCN

Laurent H. Coudert,[1] Bérenger Gans,[1] Gustavo Garcia,[2] and Jean-Christophe Loison[3]

[1)] *Institut des Sciences Moléculaires d'Orsay (ISMO), CNRS, Univ. Paris-Sud, Université Paris-Saclay, F-91405 Orsay, France*

[2)] *Synchrotron SOLEIL, L'Orme des Merisiers, Saint Aubin BP 48, F-91192 Gif sur Yvette Cedex, France*

[3)] *Institut des Sciences Moléculaires, UMR 5255 CNRS - Université de Bordeaux, Bât. A12, 351 Cours de la Libération, F-33405 Talence cedex, France*

(Dated: 10 January 2018)

The line intensity of photoelectron spectra when either the neutral or cationic species display a Renner-Teller coupling is derived and applied to the modeling of the photoelectron spectra of CNC, CCN, and HCCN. The rovibronic energy levels of these three radicals and of their cation are investigated starting from *ab initio* results. A model treating simultaneously the bending mode and the overall rotation is developed to deal with the quasilinearity problem in CNC^+, CCN^+, and HCCN and accounts for the large amplitude nature of their bending mode. This model is extended to treat the Renner-Teller coupling in CNC, CCN, and $HCCN^+$. Based on the derived photoelectron line intensity, the photoelectron spectra of all three molecules is calculated and compared to the experimental one.

I. INTRODUCTION

Photoelectron spectroscopy allows us to study complicated rovibronic transitions, between neutral and cationic species, requiring in many cases dedicated models. This is well illustrated by the photoelectron spectra of ethylene[1] and methane[2] which required new models to compute the torsional energy levels of $C_2H_4^+$ and to treat the Jahn-Teller effect in CH_4^+. This is also well illustrated by the photoelectron spectrum of acetylene[3,4] which could be analyzed once the unusual tetra-atomic Renner-Teller coupling[5] in $C_2H_2^+$ was accounted for.

Recently, the photoelectron spectra of several radicals, including CNC, CCN, and HCCN, have been reported.[6] Just as the acetylene molecule, these species or their cation display a Renner-Teller (RT) coupling, but modeling their photoionization spectra is expected to be theoretically more challenging for several reasons. A larger RT interaction characterized by a Renner parameter ϵ of the order of 0.5 in CNC and CCN, and larger than 1 in $HCCN^+$ should be accounted for. In the quasilinear CNC^+, CCN^+, and HCCN, the bending mode should be dealt with as a large amplitude motion since it is characterized by a very low frequency on the order of 100 cm^{-1}. More importantly, although theoretical calculations of the line strength of photoelectron spectra are available for diatomic[7–10] and polyatomic[1,11–15] molecules, there are no results for molecules displaying a RT coupling.

In this paper, a theoretical formalism aimed at accounting for the photoionization spectrum of non-rigid molecules displaying a RT coupling is developed and applied to the simulation of the photoelectron spectrum[6] of CNC, CCN, and HCCN. Starting from *ab initio* calculations, bending potentials were derived for these three neutral species and their cation. The rovibrational energy levels of CNC^+, CCN^+, and HCCN, characterized by a nondegenerate sigma electronic state, were computed using an approach in which the overall rotation and the large amplitude bending mode are treated simultaneously[16–21] in order to account for the quasilinearity. Using previous theoretical results,[22–27] this approach is extended to include the RT effect and allows us to retrieve the rovibronic energy levels of CNC, CCN, and $HCCN^+$. Finally, an expression for the line strength of photoelectron spectra when one of the electronic states displays the RT coupling is derived and written in terms of Franck-Condon factors involving the bending wavefunctions of the neutral and cationic species. Since none of the photoionization spectra dealt with are rotationnaly resolved,[6] only the K structure is accounted for in the energy level calculation and the line strength is averaged

over rotational levels.

These theoretical results are first applied to the ionizing transition of H_2O which provides us with a test for the theoretical approach since the cation H_2O^+ is strongly affected by the RT coupling. The threshold photoelectron spectrum (TPES), calculated from available potential energy surfaces[28,29] and using the newly derived line strength expression, compares fairly well with the experimental one.[30,31] The theoretical results are then applied to the modeling of the photoelectron spectra of CNC, CCN, and HCCN. These spectra turned out to be in good agreement with the experimental ones,[6] even for HCCN where the RT coupling in its cationic species is the largest.

This paper has five remaining sections. In Section II, the results of the *ab initio* calculations and their fitting are presented. Section III is concerned with the effective approaches used to account for the quasilinearity and the RT coupling. In Section IV, the expression of the photoionization cross section when one of the electronic states displays the RT coupling is introduced. These results are applied to H_2O, CNC, CCN, and HCCN in Section V. Section VI is the discussion.

II. *AB INITIO* CALCULATIONS

The *ab initio* calculations of the electronic states of the CNC, CCN, and HCCN radicals and their cation were carried out using the CCSD(T) (Coupled-Cluster with Single and Double and perturbative Triple excitations) method explicitly correlated (RCCSD(T)-F12) as well as internally contracted multireference configuration interaction method with Davidson correction (MRCI+Q) with complete active space self-consistent field (CASSCF) wavefunctions. All calculations were performed using the MOLPRO 2012 package and the Dunning augmented triple and quadruple zeta basis. The potential energy curves used for the photoelectron calculations are those calculated using RCCSD(T)-F12.

Ground state potential energy curves, displayed in Figs. 1, 2, and 3, were computed as a function of a bending angle denoted γ, optimizing all other structural parameters. For the triatomic CNC and CCN, γ was taken as the angle $\angle$CNC and $\angle$CCN, respectively; for the tetra-atomic HCCN, γ is the $\angle$HCC angle corresponding to the ν_5 mode.[32] We have chosen to use the curves calculated at the RCCSD(T)-F12 level rather than those at MRCI level because the geometry optimization is performed only at CASSCF for MRCI calculations.

Both methods, RCCSD(T)-F12 and MRCI, lead to very similar results. The CASSCF and MRCI calculations were performed at full valence active space for CNC and CCN, namely with 19 (18 for the cations) electrons distributed in 15 orbitals with the 1s orbitals of carbon and nitrogen atoms kept doubly occupied but fully optimized. The CASSCF and MRCI calculations were performed at smaller active space for HCCN due to convergence problems, namely with 20 (19 for $HCCN^+$) electrons distributed in 13 orbitals with the 1s and 2s orbitals of carbon and nitrogen atoms kept doubly occupied but fully optimized.

The optimized value for the geometries at the RCCSD(T)-F12/AVTZ level for CNC, CCN, and HCCN and their cation are listed in Table I where, when available, they are compared with previous experimental or theoretical values. The calculated energy differences between the cation and the neutral for the linear geometry, not given in this table, are 9.734, 10.768, 10.574 eV, for CNC, CCN, and HCCN, respectively.

Numerical values were least squares fitted to a polynomial expansion $F(\gamma)$ written in term of $\pi - \gamma$, the supplement of γ:

$$F(\gamma) = \sum_{i=0}^{n} f_i(\pi - \gamma)^i \tag{1}$$

where f_i, with $0 \leq i \leq n$, are the fitted constants. 4 such constants were retrieved for each electronic state and for each parameter allowing us to reproduce accurately the *ab initio* values. For potential energies and bond lengths, the expansion in Eq. (1) was restricted to even values of i. For a pair of RT electronic substates, the f_0 parameters of both substates were constrained to be equal to ensure the required degeneracy for the linear configuration. Due to a convergence problem, the *ab initio* calculations could not be carried out for $\gamma < \gamma_{\min}$, where the angle $\gamma_{\min}$ is between 90 and 115° depending on the species and the electronic state. In order to obtain physically meaningful results, Eq. (1) should not be used for values of γ smaller than $\gamma_{\min}$.

For the CNC radical, fitting of the *ab initio* potential energy points with the expansion in Eq. (1) yielded root-mean-square (RMS) deviations of 2.5 and 2.4 cm^{-1} for the neutral and cationic species, respectively. It was also possible to retrieve an accurate value for the Renner parameter ϵ. A value of 0.562 was obtained and turned out to be in good agreement with that reported by Merer and Travis,[34] 0.549.

Similarly for the CCN radical, the fit of the *ab initio* potential energy points led to root-mean-square (RMS) deviations of 1.5 and 26 cm^{-1} for the neutral and cationic species,

Table I. Experimental and calculated structural parameters[a]

Species	State[b]	Parameter[c]	Experimental[d]	Theory	Theory (*this work*)[e]
CNC	$X\,^2\Pi_g$	∠CNC	180[34]	180[35]	180
		r(CN)	1.245[34]	1.2534[35]	1.2462
CNC^+	$X^+\,^1\Sigma_g^+$	∠CNC		180[36,37]	180
		r(CN)		1.2427,[36] 1.2534[37]	1.2468
CCN	$X\,^2\Pi$	∠CCN	180[38]	180[35]	180
		r(CC)		1.4045,[35] 1.3749[26]	1.3821
		r(CN)		1.1889,[35] 1.1847[26]	1.1847
CCN^+	$X^+\,^1\Sigma^+$	∠CNC		180[36,37]	180
		r(CC)		1.3803,[36] 1.381[37]	1.3821
		r(CN)		1.1815,[36] 1.2534[37]	1.1906
HCCN	$X\,^3A''$	∠HCC	180[33]	144.9,[32] 137.5,[39] 144.95[40]	145.36
		∠CCN	180[33]	175.4,[32] 175.6,[39] 175.45[40]	175.26
		r(HC)	0.998[33]	1.069,[32] 1.063,[39] 1.0689[40]	1.0707
		r(CC)	1.323[33]	1.328,[32] 1.372,[39] 1.3267[40]	1.3285
		r(CN)	1.195[33]	1.186,[32] 1.184,[39] 1.1850[40]	1.1898
$HCCN^+$	$X^+\,^2A'$	∠HCC		152.7[39]	163.59
		∠CCN		174.1[39]	175.92
		r(HC)		1.095[39]	1.0842
		r(CC)		1.317[39]	1.2981
		r(CN)		1.212[39]	1.2048
	$A^+\,^2A''$	∠HCC		180[39]	180
		∠CCN		180[39]	180
		r(HC)		1.092[39]	1.083
		r(CC)		1.300[39]	1.291
		r(CN)		1.219[39]	1.207

[a] Bond lengths are in Å and bond angles in degrees.

[b] In CNC, the RT coupling leads to lower $^2A_2$ and upper $^2B_2$ substates; for CCN, to lower $^2A''$ and upper $^2A'$ substates; and for $HCCN^+$ to lower $^2A'$ and upper $^2A''$ substates.

[c] For HCCN and $HCCN^+$ the dihedral ∠HCCN is 180°, consistent with trans conformations.

[d] For HCCN, Brown *et al.*[33] assumed a linear geometry.

[e] Obtained at the RCCSD(T)-F12/AVTZ level of theory.

respectively. The value obtained for the Renner parameter ϵ, 0.424, is in reasonable agreement with that reported by Merer and Travis,[38] 0.44, but in better agreement with that calculated by Hill *et al.*,[26] 0.429. It is in poor agreement with that retrieved by Kohguchi

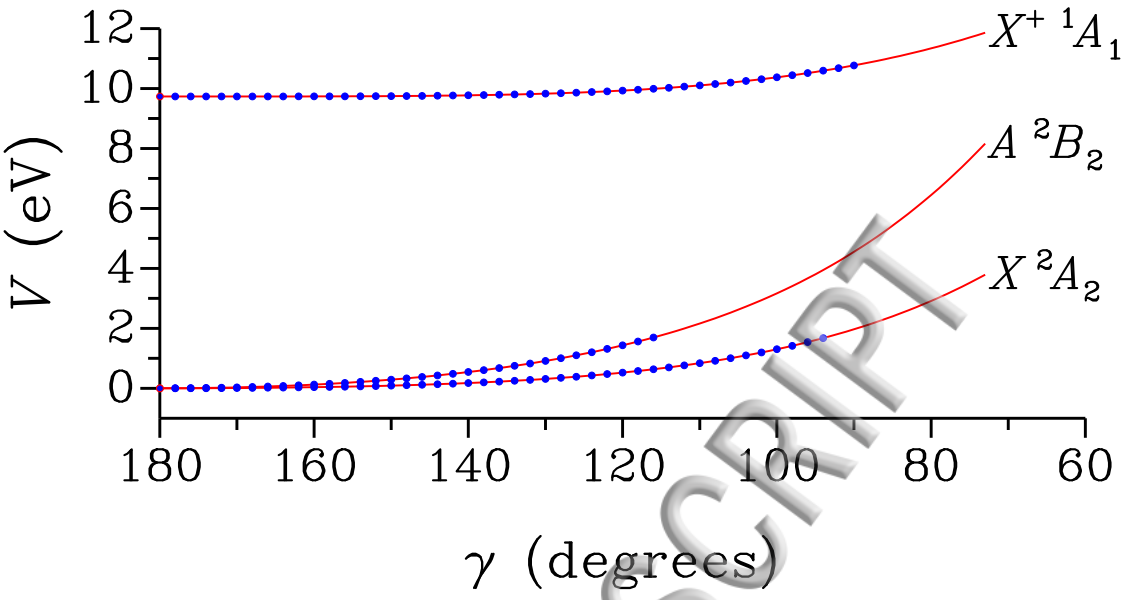

Figure 1. Variations with the bending angle $\gamma = \angle$CNC of the potential energy function V in eV for the $X\,^2A_2$ and $A\,^2B_2$ electronic substates of the CNC radical resulting from the RT coupling and for the $X\,^1A_1$ electronic state of the CNC^+ cation. *Ab initio* potential values are indicated by dots. Solid lines are the fitted bending potentials calculated with Eq. (1).

et al.,[41] 0.489.

As can be seen in Table I, the HCCN radical and the $HCCN^+$ cation display a nearly linear equilibrium geometry. The *ab initio* calculations also confirm that the neutral and cationic species are planar[32,39,40] and that when $\gamma = 180°$, the bending angle $\beta = \angle$CCN is 180°. When fitting the *ab initio* values of this angle, the angle supplement $\pi - \beta$ was fitted to the expansion of Eq. (1) which was restricted to odd values of i. This ensures the required linearity for $\gamma = 180°$. The angle β is plotted in Fig. 4 as a function of γ. For $\gamma \geq 110°$, the results are consistent with the molecule assuming a Z-shaped trans geometry for the $X\,^3A''$ electronic state of the neutral radical and the $X^+\,^2A'$ electronic substate of the cation as the dihedral angle $\angle$HCCN is 180°. For the $A^+\,^2A''$ electronic substate, the angle β displays almost no change and remains close to 180°. The RMS deviations of the fits of the *ab initio* potential energy points are 12 and 4.1 cm^{-1} for the neutral and the cationic species, respectively.

The results of the fit of the *ab initio* bond lengths with the polynomial expansion in Eq. (1) is summarized for all species in the form of figures available as supplementary material.

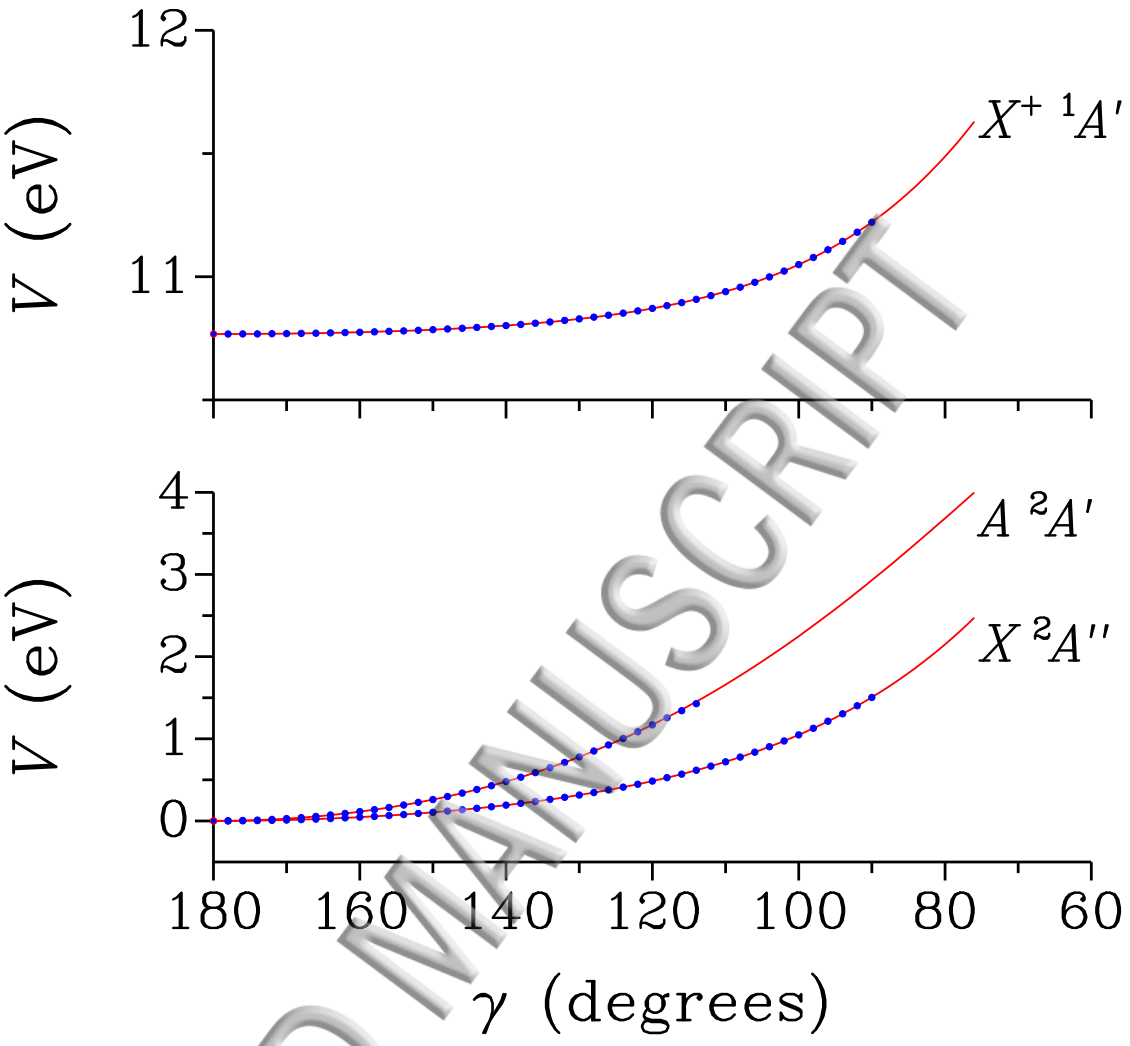

Figure 2. Variations with the bending angle $\gamma = \angle$CCN of the potential energy function V in eV for the $X\,^2A''$ and $A\,^2A'$ electronic substates of the CCN radical resulting from the RT coupling and for the nondegenerate $X\,^1A'$ electronic state of the CCN^+ cation. *Ab initio* potential values are indicated by dots. Solid lines are the fitted bending potentials calculated with Eq. (1).

III. EFFECTIVE BENDING AND RT HAMILTONIANS

The systems dealt with in the present work display either a quasilinearity problem like the CNC^+ and CCN^+ cations,[36] and the HCCN radical[32,42] or a strong RT effect like the CNC and CCN radicals,[26,34,38] and the $HCCN^+$ cation.[39] In this section, effective Hamiltonians are introduced to deal with both effects and account simultaneously for the large amplitude bending mode and the overall rotation.

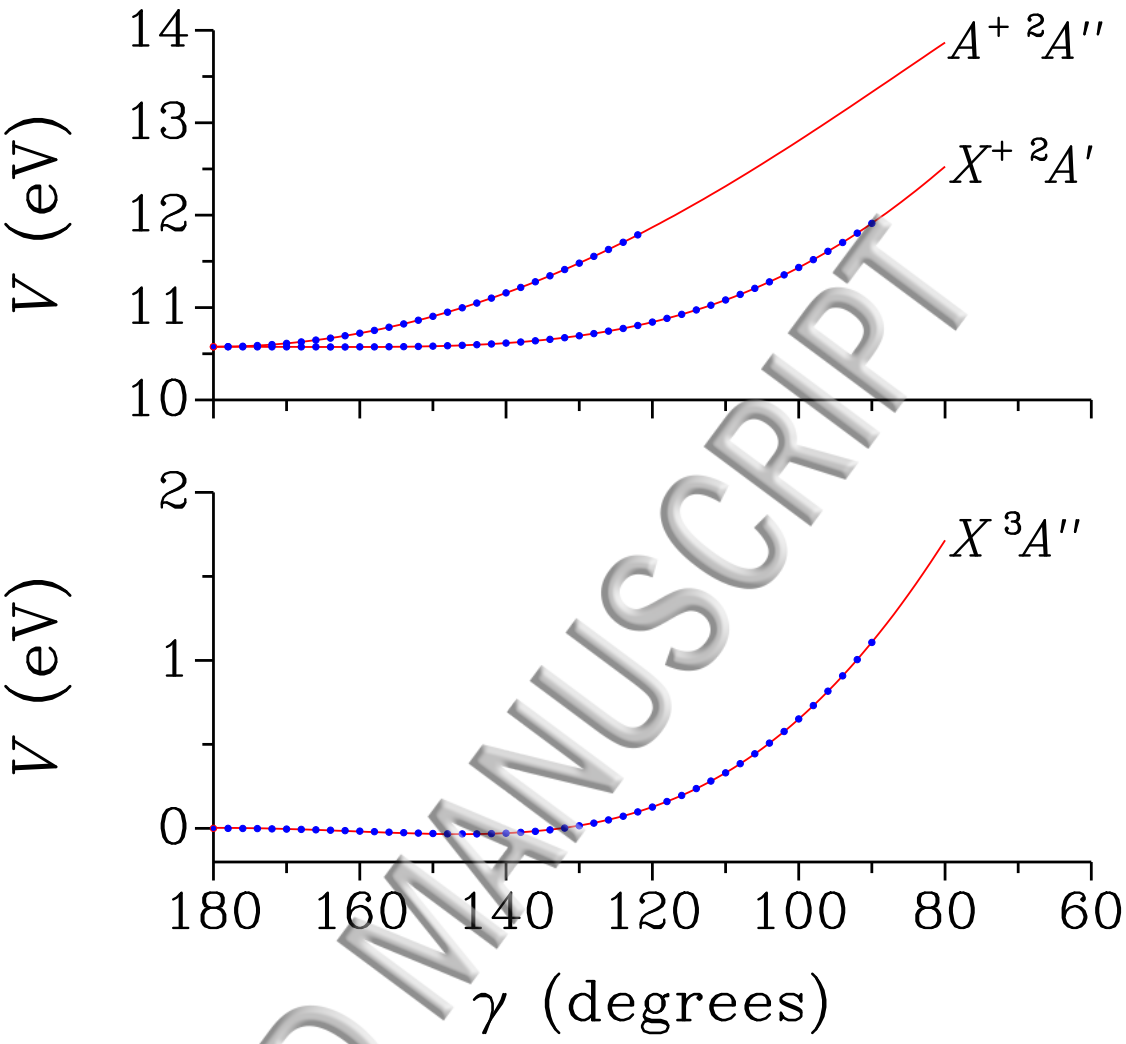

Figure 3. Variations with the bending angle $\gamma = \angle$HCC of the potential energy function V in eV for the $X^+\,^2A'$ and $A^+\,^2A''$ electronic substates of the $HCCN^+$ cation resulting from the RT coupling, top panel, and for the nondegenerate $X\,^3A''$ electronic state of the HCCN radical, bottom panel. *Ab initio* potential values are indicated by dots. Solid lines are the fitted bending potentials calculated with Eq. (1).

A. Effective bending Hamiltonian

The effective bending-rotation Hamiltonian $H_{\text{b-r}}$ introduced to treat the quasilinearity accounts for the large amplitude nature of the bending mode and relies on the Bending-Rotation approach[16–21] developed to deal with the anomalous centrifugal distortion of the water molecule.[43] The Bending-Rotation approach[16–21] accounts exactly for the fact that the A rotational constant goes to infinity for the linear configuration.

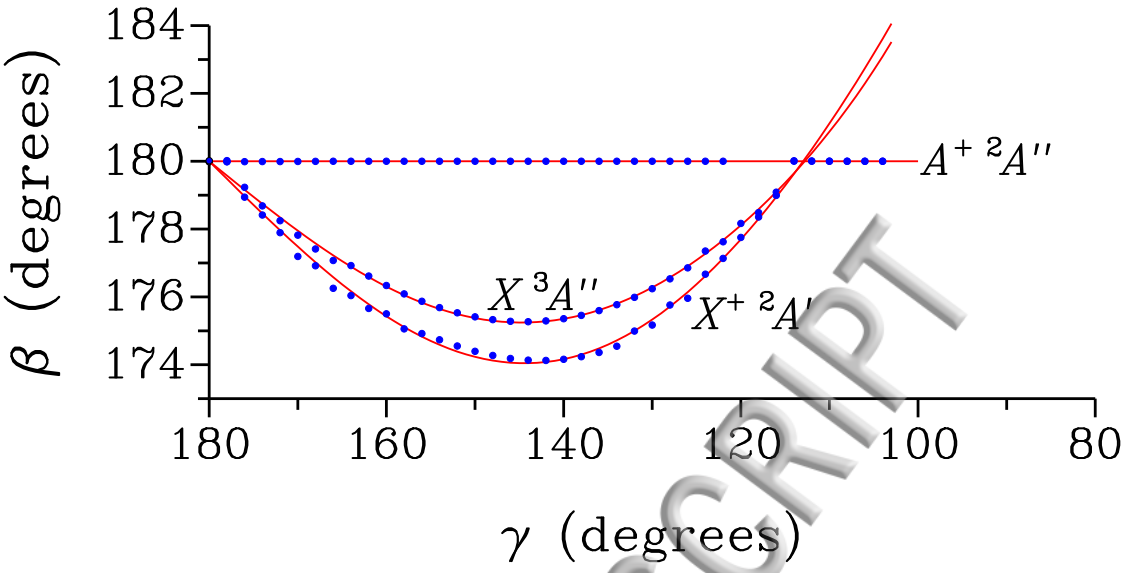

Figure 4. Variations with the bending angle $\gamma = \angle$HCC of the angle $\beta = \angle$CCN in degrees for the $X\,^2A''$ and $A\,^2A'$ electronic substates of the $HCCN^+$ cation and for the $X\,^3A''$ electronic state of the HCCN radical. *Ab initio* values are indicated by dots. Solid lines are fitted values calculated with Eq. (1).

$H_{\text{b-r}}$ is written in term of the large amplitude coordinate $t = \cos\gamma$. Following Hougen *et al.*[44] and Mekhtiev *et al.*,[45] a reference configuration represented by atom positions $\mathbf{a}_i(t)$ is used and a four-dimensional effective Hamiltonian describing the large amplitude bending motion and the overall rotation is derived. A molecule fixed xyz axis system is chosen such that its origin is the molecular center of mass, its xz plane is the molecular plane, and the molecule is along the z axis for the $t = -1$ linear configuration. Obtaining atom positions $\mathbf{a}_i(t)$ and their derivatives $\partial\mathbf{a}_i(t)/\partial t$ from Section II, the 4×4 symmetrical generalized inertia tensor[44] $\mathbf{I}(t)$ is computed using Eqs. [5] of Mekhtiev *et al.*[45] The effective Hamiltonian $H_{\text{b-r}}$ is then expressed with the generalized inverse inertia tensor[44,45] $\boldsymbol{\mu}(t) = [\mathbf{I}(t)]^{-1}$ as:

$$\begin{aligned} H_{\text{b-r}} &= \tfrac{1}{2}P_t\mu_{tt}(t)P_t + \tfrac{1}{2}\sum_{\delta=x,y,z}\mu_{\delta\delta}(t)N_\delta^2 \\ &+ \tfrac{1}{2}\mu_{xz}(t)\{N_x, N_z\} + \tfrac{1}{2}\{\mu_{yt}(t), P_t\}N_y + V(t), \end{aligned} \tag{2}$$

where $\mu_{tt}(t)$, $\mu_{xx}(t)$, $\mu_{yy}(t)$, $\mu_{zz}(t)$, $\mu_{xz}(t)$, and $\mu_{yt}(t)$ are components of the generalized inverse inertia tensor;[44,45] $\{,\}$ is the anticommutator; P_t is the momentum conjugate to t; N_δ, with $\delta = x, y, z$, are molecule fixed components of the rotational angular momentum $\mathbf{N}$; and $V(t)$ is the potential energy function. In Eq. (2), only two non-diagonal components

of the generalized inverse inertia tensor arise due to the symmetry plane. A term involving the determinant of the $\boldsymbol{\mu}(t)$ tensor giving rise to a mass dependent potential analogous to those in Eq. (36) of Hougen *et al.*[44] and in Eq. [10] of Mekhtiev *et al.*[45] has been omitted in Eq. (2). The volume element to be used for the effective Hamiltonian $H_{\text{b-r}}$ is $\sin\theta \mathrm{d}\theta\mathrm{d}\phi\mathrm{d}\chi\mathrm{d}t$.

Although there are no analytical expression for the components of the generalized inverse inertia tensor, in the linear limit, when $t \to -1$, the two non-diagonal components $\mu_{xz}(t)$ and $\mu_{ty}(t)$ go to zero and the four diagonal components display the following behavior:

$$\lim_{t\to-1} \begin{cases} \mu_{zz}(t) = \dfrac{A}{1+t}, & \mu_{xx}(t) = 2B, \\ \mu_{tt}(t) = 2B_e(1-t^2), & \mu_{yy}(t) = 2B, \end{cases} \tag{3}$$

where A, B_e, and B are three kinetic energy parameters. Although the meaning of A and B_e is not obvious, B clearly is the rotational constant of the linear configuration. The results in Eqs. (3) are well illustrated by the CNC^+ cation. Taking into account the above requirements, the molecule fixed axis system is attached to the molecule so that its x axis bisects the $\angle$CNC bending angle. Figure 5 depicts the variations of $\mu_{tt}(t)/(1-t^2)$, $\mu_{xx}(t)$, $\mu_{yy}(t)$, and $(1+t)\mu_{zz}(t)$. All the curves in this figure display a smooth behavior and it can be deduced that $A = B_e = 4.9$ cm^{-1} and $B = 0.451$ cm^{-1}.

Equations (3) mean that when $t \to -1$, the limiting behavior of the terms in the effective Hamiltonian of Eq. (2) is the same as those in the Bending-Rotation Hamiltonian defined in Eqs. (1)–(3) of Coudert.[16] This suggests that the Schrödinger equation for the bending mode should be solved using the same $\theta_n^{\alpha\beta}(t)$ basis set functions:

$$\theta_n^{\alpha\beta}(t) = (1-t)^{\alpha/2}(1+t)^{\beta/2}P_n^{(\alpha,\beta)}(t)/\sqrt{h_n}, \tag{4}$$

where n is an integer with $0 \le n \le n_{\text{Max}}$; $P_n^{(\alpha,\beta)}(t)$, with $\alpha, \beta \ge -1$, is a Jacobi polynomial;[46] and h_n is a normalizing factor given in Table 22.2 of Abramovitz and Stegun's book[46] and in Eq. (8) of Coudert.[16]

The Schrödinger equation for the effective Hamiltonian in Eq. (2) is solved[16–21] using rovibrational wavefunctions of the form:

$$\psi^{N,k}(t)|N,k\rangle, \tag{5}$$

where $\psi^{N,k}(t)$ is a vibrational bending wavefunction and $|N,k\rangle$ is a symmetric top rotational function defined as in Wigner[47] and characterized by N the quantum number of the total

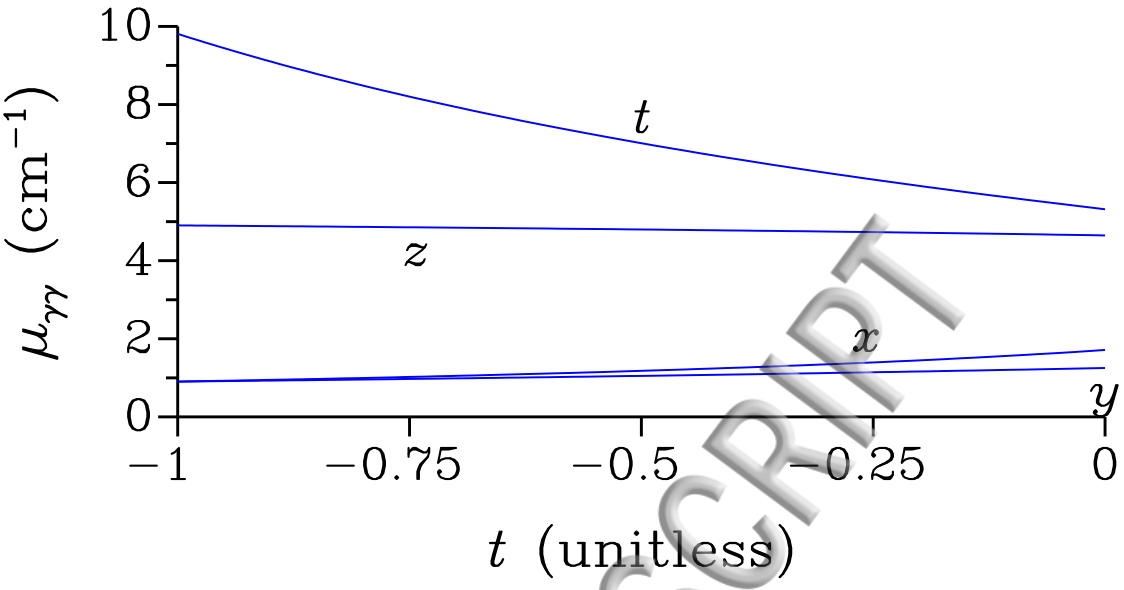

Figure 5. Variations with the unitless large amplitude coordinate t of the 4 diagonal components $\mu_{\delta\delta}(t)$ of the generalized inverse inertia tensor of the CNC^+ cation as computed from Section II. The curve identified by t, x, y, and z are respectively $\mu_{tt}(t)/(1-t^2)$, $\mu_{xx}(t)$, $\mu_{yy}(t)$, and $(1+t)\mu_{zz}(t)$ in cm^{-1}.

angular momentum and by k the eigenvalue of its molecule fixed component N_z. The symmetric top rotational function depends also on M, the eigenvalue of the laboratory fixed component N_Z, but this quantum number is omitted as the energy does not depend on M. The vibrational bending wavefunction $\psi^{N,k}(t)$ is a solution of the Schrödinger equation for the bending Hamiltonian:

$$H_{\rm b}^{N,k} = \tfrac{1}{2}P_t\mu_{tt}(t)P_t + \tfrac{1}{2}k^2\mu_{zz}(t) + V(t) + \tfrac{1}{4}[N(N+1)-k^2][\mu_{xx}(t)+\mu_{yy}(t)]. \quad (6)$$

The matrix of the bending Hamiltonian in Eq. (6) is set up and diagonalized taking the basis set functions in Eq. (4) with β such that:[16–21]

$$\beta^2 = k^2 \lim_{t\to-1} \frac{4\mu_{zz}(t)(1+t)^2}{\mu_{tt}(t)}. \quad (7)$$

This choice accounts for the singularity of the bending Hamiltonian $H_{\rm b}^{N,k}$ for the linear configuration and ensures that the basis set functions in Eq. (4) are eigenfunctions of $H_{\rm b}^{N,k} - V(t)$ when t is close to -1. In the case of the C_{2v} symmetry CNC^+ cation, Eq. (7) leads to $\beta = |k|$. The value of α can be estimated matching the $n = \beta = 0$ basis set function of

Eq. (4) with the ground state eigenfunction of the harmonic oscillator bending Hamiltonian. This leads to:

$$\alpha = 4\sqrt{f_2/B_e}, \tag{8}$$

where f_2 is the $i = 1$ expansion coefficient of the potential energy function with Eq. (1) and B_e is defined in Eqs. (3). Using the results of Section II in the case of the CCN^+ cation, we obtain $B_e = 5.01$ and $f_2 = 475$ cm^{-1} leading to $\alpha = 39$. With such a value, the basis set functions of Eq. (4) with $n \leq 10$ are vanishingly small outside the range $-1 \leq t \leq 0.5$, that is, $60° \leq \gamma \leq 180°$.

The matrix elements of the operators in Eq. (6) between two basis set functions of Eq. (4) were computed using Gaussian quadrature and accounting for the singularity of $\mu_{zz}(t)$ and $P_t\mu_{zz}(t)P_t$ at $t = -1$. For the former operator, the singularity is due to its behavior in the linear limit, described by Eqs. (3). For the latter operator, as revealed by Eq. (A2), the singularity arises because of the form of the basis set functions. A P-point Gauss-Jacobi quadrature suited for a weight function of the form $(1-t)^{\alpha'}(1+t)^{\beta'}$ was used. As shown by Eqs. (A4)–(A6), taking $\alpha' = \alpha - 1$ and $\beta' = \beta - 1$ accounts for both singularities and ensures the best accuracy.

Equation (8) puts an upper bound for the node values t_i of the quadrature. When $P = 21$, $\alpha = 39$, and $\beta = 0$, as obtained for the CCN^+ cation, the largest (smallest) value of t_i (γ_i) is 0.40 (66.4°). This means that values of γ, with $\gamma < \gamma_{\min}$, for which the results in Section II are not valid, will not be used. This provides us with an alternative way of choosing α.

Bending-rotation energies and eigenfunctions of the Hamiltonian in Eq. (2) will be written:

$$E(v, N, k) \quad \text{and} \quad \Psi^{v,N,k} = \psi_v^{N,k}(t)|N, k\rangle, \tag{9}$$

where v is the bending quantum number and $\psi_v^{N,k}(t)$ is the corresponding eigenfunction. Symmetry adapted bending-rotation wavefunctions for the C_s symmetry group can be built starting from Eq. (9), using the invariance of the bending Hamiltonian in Eq. (6) under the transformation $k \to -k$, and remembering that the effects of the inversion operation E^* of C_s on a symmetric top rotational function[48] are $E^*|N, k\rangle = (-1)^{N+k}|N, -k\rangle$. Using Wang-type rotational wavefunctions:

$$|NK\delta\rangle = (|N, K\rangle + \delta|N, -K\rangle)/\sqrt{2(1+\delta_{K,0})}, \tag{10}$$

where $K \geq 0$ and $\delta = \pm 1$, the symmetry adapted wavefunctions take the form:

$$\Psi^{v,N,K,\delta} = \psi_v^{N,K}(t)|NK\delta\rangle. \tag{11}$$

These wavefunctions belong to the symmetry species A' and A'' of C_s when $\delta(-1)^{N+K}$ is $+1$ or -1, respectively. The symmetry species of the rovibronic wavefunction should be calculated replacing this term by $\delta(-1)^{N+K}g(X\,\Sigma)$, where the $g(X\,\Sigma)$ depends on the C_s symmetry species of the nondegenerate $X\,\Sigma$ electronic state and is $+1$ (-1) for an A' (A'') electronic state.

B. Effective RT Hamiltonian

The RT effect in systems with a nonzero projection $\Lambda = 1$ of the molecule fixed component L_z of the electronic angular momentum $\mathbf{L}$ are considered. The two RT electronic substates that become degenerate in the linear limit belong to the A' and A'' symmetry species of C_s and their potential energy functions, denoted $V'(t)$ and $V''(t)$, respectively, can be obtained from Section II. In the present treatment, we only consider the large amplitude bending mode, the electron spin is ignored, and we use most of the results in Section III A. The molecule fixed axis system is attached to the molecule in the same way and a unique reference configuration is chosen for both electronic substates. The corresponding atom positions $\mathbf{a}_i(t)$ are determined from the results of Section II and calculated from internal coordinates taken as the average of the A' and A'' substates values. This choice leads to a single generalized inertia tensor calculated as in the previous section. In agreement with previous investigations,[22–27] we use electronic wavefunctions of the form $|\pm\Lambda\rangle = (|A'\rangle \pm i|A''\rangle)/\sqrt{2}$ which, in the linear limit, are eigenfunctions of L_z with eigenvalues $\pm\Lambda$. The Schrödinger equation for the effective RT Hamiltonian used in this investigation is solved using rovibronic wavefunctions of the form:

$$\psi^{+\Lambda,N,k}(t)|+\Lambda\rangle|N,k\rangle + \psi^{-\Lambda,N,k}(t)|-\Lambda\rangle|N,k\rangle, \tag{12}$$

where $|N,k\rangle$ are symmetric top rotational functions defined as for Eq. (5) and $\psi^{\pm\Lambda,N,k}(t)$ are two vibrational functions. For this pair of functions the Schrödinger equation is expressed as a 2×2 matrix:

$$\begin{pmatrix} H_b^{+\Lambda,N,k}(t) & V_-(t) \\ V_-(t) & H_b^{-\Lambda,N,k}(t) \end{pmatrix}, \tag{13}$$

where $H_b^{\pm\Lambda,N,k}(t)$ are vibrational operators and $V_-(t) = [V'(t) - V''(t)]/2$. Neglecting the geometry variations of the expectation value of L_z and L_z^2, the vibrational operators $H_b^{\pm\Lambda,N,k}(t)$ take the following form:[22–27]

$$\begin{aligned} H_b^{\pm\Lambda,N,k} &= \tfrac{1}{2} P_t \mu_{tt}(t) P_t + \tfrac{1}{2}(k \pm \Lambda)^2 \mu_{zz}(t) \\ &+ \tfrac{1}{4}[N(N+1) - k^2][\mu_{xx}(t) + \mu_{yy}(t)] + V_+(t), \end{aligned} \tag{14}$$

where $\mu_{\delta\delta}(t)$, with $\delta = t, x, y, z$, are diagonal components of the generalized inertia tensor and $V_+(t) = [V'(t) + V''(t)]/2$.

The matrix of the Hamiltonian in Eq. (13) is set up and diagonalized expanding the vibrational functions $\psi^{\pm\Lambda,N,k}(t)$ in terms of the basis set functions of Eq. (4). The corresponding values of α and β are denoted $\alpha^\pm$ and $\beta^\pm$. As Eqs. (3) are also valid, an equation similar to Eq. (7) holds:

$$\beta^{\pm 2} = (k \pm \Lambda)^2 \lim_{t \to -1} \frac{4\mu_{zz}(t)(1+t)^2}{\mu_{tt}(t)}. \tag{15}$$

The value of $\alpha^\pm$ can be estimated from the potential energy functions of the A' and A'' substates. Using Eq. (14), an equation similar to Eq. (8) arises:

$$\alpha^\pm = 4\sqrt{f_2^+ / B_e}, \tag{16}$$

where f_2^+ is the average value of the f_2 expansion coefficients of Eq. (1) for the potential energy function of the A' and A'' substates; and where B_e is defined in Eqs. (3). Evaluation of the matrix elements needed to set up the matrix of the Hamiltonian in Eq. (13) should be carried out as in Section III A. For $H_b^{\pm\Lambda,N,k}(t)$, Eqs. (A4)–(A6) should be used; for the potential energy function term $V_-(t)$, the Gauss-Jacobi quadrature for the weight function $(1-t)^{(\alpha^+ + \alpha^-)/2}(1+t)^{(\beta^+ + \beta^-)/2}$ should be utilized.

Symmetry adapted rovibronic functions for the C_s point group, denoted $\Psi^{v,\Lambda,N,K,\delta}$, where v is the bending quantum number, $K \geq 0$, and $\delta = \pm 1$, are expressed in terms of the electronic wavefunctions of the A' and A'' substates; and of the Wang-type rotational functions $|NK\delta\rangle$ of Eq. (10) as:

$$\begin{aligned} &\Psi^{v,\Lambda,N,K,\delta} = \\ &\frac{1}{\sqrt{2}}\{|A'\rangle[\psi_v^{+\Lambda,N,K}(t) + \psi_v^{-\Lambda,N,K}(t)]|NK\delta\rangle \\ &+ i|A''\rangle[\psi_v^{+\Lambda,N,K}(t) - \psi_v^{-\Lambda,N,K}(t)]|NK{-}\delta\rangle\}, \end{aligned} \tag{17}$$

where $\psi_v^{+\Lambda,N,K}(t)$ and $\psi_v^{-\Lambda,N,K}(t)$ are solutions of Eq. (13) characterized by the bending quantum number v and fulfilling:

$$\int_{-1}^{+1} dt \, \{|\psi_v^{+\Lambda,N,K}(t)|^2 + |\psi_v^{-\Lambda,N,K}(t)|^2\} = 1. \tag{18}$$

The wavefunctions in Eq. (17) belong to the symmetry species A' and A'' of C_s when $\delta(-1)^{N+K}$ is $+1$ or -1, respectively. This equation is physically more meaningful than Eq. (12) because it is expressed in terms of the actual $|A'\rangle$ and $|A''\rangle$ electronic wavefunctions of the RT substates.

IV. RT COUPLING AND PHOTOIONIZATION CROSS SECTION

Theoretical calculations of the photoionization cross section were performed for diatomic[7–10] and polyatomic[1,11–15] molecules. Simplified results are available for molecules displaying the RT coupling.[22,49] In this work the results derived by Willitsch *et al.*[15] for an asymmetric-top polyatomic molecule are used. The photoionization cross section derived by these authors is given in the first of their Eqs. (7). This equation, obtained ignoring the electron spin, involves electronic and rovibrational terms. The latter, given in the second of their Eqs. (7), consists of a Franck-Condon factor $(q_v)^2 = |\langle v^+|v''\rangle|^2$ and a rotational factor $Q(l'')$. These factors are evaluated in this section when the neutral and cationic species are described by the large amplitude approaches introduced in Section III.

A. RT coupling in the $X\,\Pi$ state of the neutral species

The electronic state of the cation, denoted $X^+\,\Sigma$, is then either an A' or A'' state. The results of Willitsch *et al.*[15] are used to calculate the total photoionization cross section $\sigma_{\rm tot}$ of the $X^+\,\Sigma \leftarrow X\,\Pi$ ionizing transition by adding the contribution of each RT component. Below, these contributions are distinguished using a $\pm$ sign where the upper (lower) sign is for the $X^+\,\Sigma \leftarrow X\,A'$ ($X^+\,\Sigma \leftarrow X\,A''$) transition. For either component, the lower level labeled v'', N'', K'', δ'' is described by the wavefunction in Eq. (17) and connects to the upper level of the cation labeled v^+, N^+, K^+, δ^+ described by the wavefunction in Eq. (11). It can

be shown that the following Franck-Condon factor arises:

$$(q_v^{\pm})^2 = \left| \int_{-1}^{+1} \psi_{v^+}^{N^+,K^+}(t)[\psi_{v''}^{+\Lambda,N'',K''}(t) \pm \psi_{v''}^{-\Lambda,N'',K''}(t)]dt \right|^2, \tag{19}$$

where the vibrational wavefunctions $\psi_{v^+}^{N^+,K^+}(t)$ and $\psi_{v''}^{\pm\Lambda,N'',K''}(t)$ should be taken from Eqs. (9) and (12), respectively. The $Q(l'')$ factor can be written:

$$\begin{aligned} Q^{\pm}(l'') = (2N^+ + 1) \Bigg[& \begin{pmatrix} N^+ & l'' & N'' \\ -K^+ & \lambda'' & K'' \end{pmatrix} \\ & \pm \delta'' \begin{pmatrix} N^+ & l'' & N'' \\ -K^+ & \lambda'' & -K'' \end{pmatrix} + \delta^{\pm} \begin{pmatrix} N^+ & l'' & N'' \\ K^+ & \lambda'' & K'' \end{pmatrix} \\ & \pm \delta^+\delta'' \begin{pmatrix} N^+ & l'' & N'' \\ K^+ & \lambda'' & -K'' \end{pmatrix} \Bigg]^2 / h(K^+, K''). \end{aligned} \tag{20}$$

where $h(K^+, K'') = 4(1 + \delta_{K^+,0})(1 + \delta_{K'',0})$. Taking into account the electronic terms and the contributions from both RT components, the total cross section can be written:[15]

$$\begin{aligned} \sigma_{\text{tot}} = \rho''[(q_v^+)^2 & \sum_{|\lambda''| \le l''} \frac{Q^+(l'')B_{l''\lambda''}^{(A')}}{2l''+1} \\ & + (q_v^-)^2 \sum_{|\lambda''| \le l''} \frac{Q^-(l'')B_{l''\lambda''}^{(A'')}}{2l''+1}]/2, \end{aligned} \tag{21}$$

where the electronic terms $B_{l''\lambda''}^{(A')}$ and $B_{l''\lambda''}^{(A'')}$ are defined in Eq. (10) of Willitsch *et al.*[15] and correspond to either RT electronic substates; and ρ'' is a weighing factor depending on the lower level. The Franck-Condon factors in Eq. (21) should be calculated with a Gauss-Jacobi quadrature. Symmetry considerations based on the nature of the partial wave describing the photoelectron[13,15] put some restrictions on the quantum numbers of the upper and lower levels. Equation (3) of Willitsch *et al.*[15] and the results at the end of Sections III A and III B lead to:

$$\delta^+(-1)^{N^+ + K^+} g(X^+\,\Sigma)\, \delta''(-1)^{N'' + K''} = -(-1)^l, \tag{22}$$

where l is the orbital angular momentum of the photoelectron partial wave.

Since the rotational structure is not expected to be resolved in the photoionization spectrum of the heavy molecules studied in this work, the cross section should be averaged over

rotational levels. It will be averaged over N^+ and N'', but not over v^+, K^+ and v'', K'' as resolved vibrational and K structure might be observed. The averaged cross section will be calculated as:

$$\sigma_{\rm tot}^{\rm vib}(v^+, K^+ \leftarrow v'', K'') = \sum_{N'',\delta''} \sum_{N^+,\delta^+} \sigma_{\rm tot}. \tag{23}$$

Using the same ideas as in Section 5 of Buckingham *et al.*[7] and neglecting in Eq. (19) the dependence of the Franck-Condon factors on N^+ and N'', evaluation of the summation over the rotational quantum numbers of the upper level N^+ and δ^+ leads to:

$$\sum_{N^+,\delta^+} Q^{\pm}(l'') = (\delta_{K^+,|K''+\lambda''|} + \delta_{K^+,|K''-\lambda''|})/4, \tag{24}$$

where N^+ and δ^+ are such that Eq. (22) is fulfilled and λ'' is nonzero. As the result in Eq. (24) does not depend on the rotational quantum numbers of the lower level, N'' and δ'', the summation over these quantum numbers in Eq. (23) reduces to:

$$\begin{aligned} \sum_{N'',\delta''} \rho'' &= \exp[-E_{\rm rv}(v'', K'')/kT] Z_{\rm r}/Z \\ &= \rho''(v'', K'') Z_{\rm r}/Z, \end{aligned} \tag{25}$$

where Z is the partition function of the molecule; T the temperature; k the Boltzmann constant; $E_{\rm rv}(v'', K'')$ the rovibrational energy; and $Z_{\rm r}$ the rotational partition function. This partition function is assumed to be independent of v'' and K'' and to depend only on the temperature. The averaged cross section can now be written:

$$\begin{aligned} \sigma_{\rm tot}^{\rm vib}(v^+, K^+ \leftarrow v'', K'') &= \rho''(v'', K'') Z_{\rm r}/Z \\ &\times \sum_{|\lambda''| \le l''} [(q_v^+)^2 B_{l''\lambda''}^{(A')} + (q_v^-)^2 B_{l''\lambda''}^{(A'')}]/(2l''+1) \\ &\times (\delta_{K^+,|K''+\lambda''|} + \delta_{K^+,|K''-\lambda''|})/8. \end{aligned} \tag{26}$$

When using this equation, rovibrational energies for given v and K values should be computed setting N equal to K in Eqs. (6) and (14). The vibrational functions thus obtained should be used to obtain the Franck-Condon factors.

B. RT coupling in the $X^+\,\Pi$ state of the cationic species

The electronic state of the neutral, denoted $X\,\Sigma$, is then either an A' or A'' state. The total photoionization cross section $\sigma_{\rm tot}$ of the $X^+\,\Pi \leftarrow X\,\Sigma$ ionizing transition is obtained

by adding the contribution of the RT components $X^+\,A' \leftarrow X\,\Sigma$ and $X^+\,A'' \leftarrow X\,\Sigma$ distinguished using + and − signs, respectively. The resulting total and averaged photoionization cross section can be obtained making a few changes in Section IV A. In Eqs. (21) and (26), the electronic terms $B^{(A')}_{l''\lambda''}$ and $B^{(A'')}_{l''\lambda''}$ should be both replaced by $B^{(X)}_{l''\lambda''}$. The Franck-Condon factor $(q^{\pm}_v)^2$ should be evaluated making the substitution $v'', N'', K'' \leftrightarrow v^+, N^+, K^+$ in Eq. (19). In the rotational factor $Q(l'')$ of Eq. (20), the substitutions $\delta'' \rightarrow \pm\delta''$ and $\delta^+ \rightarrow \pm\delta^+$ should be made. At last in Eq. (22), $g(X^+\,\Sigma)$ becomes $g(X\,\Sigma)$.

For the molecules dealt with in the present investigation, the photoelectron is ejected from a π orbital. This means that $\lambda'' = 1$. In Eqs. (21) and (26), the first term in the summation over l'' will be assumed to be the dominant term and this summation will be restricted to the $l'' = 1$ term. It will also be assumed that electronic terms $B^{(A')}_{l''\lambda''}$ and $B^{(A'')}_{l''\lambda''}$ of Section IV A are equal.

V. NUMERICAL RESULTS

Using the two previous sections, photoionization cross sections are calculated for the ionizing transitions of H_2O, CNC, CCN, and HCCN. The first molecule provides us with a test of the theoretical approach and also allows us to understand the contribution of the various terms in Eq. (26) to the TPES. For the three remaining molecules, comparisons with the experimental photoionization spectra[6] are carried out. With the experimental setup used in this reference, the energy resolution is 17 meV and the rotational temperature, fairly well known, is around 200 K. The vibrational temperature is, however, not as well defined and can be quite high since the consecutive $R{-}H + F \longrightarrow R + HF$ reactions are exothermic. Below, we have chosen a temperature of 500 K for the simulations of the CNC, CCN, and HCCN spectra.

A. Neutral H_2O and H_2O^+ cation

Starting from the potential energy surfaces of Partridge and Schwenke[28] for the neutral species and of Wu *et al.*[29] for the cation, bending potentials and bond lengths were retrieved for the ground stretching states. The results of Sections III A and III B were then applied to the calculation of the rovibronic energies of H_2O and H_2O^+. A sufficient accuracy was

Table II. Calculated rovibronic energies[a] for H_2O and H_2O^+

State[b]	v_2	K	Cal.[c]	Cal.[d]
$X\,^1A_1$	0	1	39.7	39.2
	1	0	1594.3	1587.6
	1	1	1637.5	1630.3
	2	0	3151.7	3143.2
	2	1	3199.5	3190.7
	3	0	4666.1	4660.9
	3	1	4720.8	4715.5
$X^+\,^2B_1$	0	1	37.3	38.8
	1	0	1417.8	1410.0
	1	1	1459.2	1452.9
	2	0	2784.4	2776.2
	2	1	2831.7	2825.0
	3	0	4097.3	4092.9
	3	1	4153.1	4150.3
$A^+\,^2A_1$	0	0	8379.5	8381.9
	0	1	9033.9	9006.2
	1	0	9884.6	9901.0
	1	1	10647.1	10654.8
	2	0	11564.3	11605.8
	2	1	12498.4	12563.9

[a] Levels are identified by their electronic state, the bent molecule vibrational quantum number v_2, and the rotational quantum number K as defined in Sections III A and III B.

[b] $X\,^1A_1$ is the ground electronic state of H_2O, $X^+\,^2B_1$ and $A^+\,^2A_1$ are respectively lower and upper RT substates of H_2O^+.

[c] Energy in cm^{-1} calculated by Bunker and Stone[50] for H_2O and Wu *et al.*[29] for H_2O^+. For $K = 1$, the average value of the K-type doublet was taken.

[d] Energy in cm^{-1} calculated in Section V A taking the same energy origin as Bunker and Stone,[50] and Wu *et al.*[29]

reached setting n_{Max}, the maximum value of n for the basis set functions in Eq. (4), to 30, P the number of points of the Gauss-Jacobi quadrature to 33, and $\alpha, \alpha^{\pm}$ to 10. Table II displays a comparison between the present results and those previously calculated.[29,50] For H_2O, the discrepancies range from 0 to 10 cm^{-1}. For H_2O^+ the discrepancies are larger, especially for the $A^+\,^2A_1$ state, but the theoretical approach reproduces well the large energy increase when K goes from 0 to 1.

The photoionization cross sections were calculated with Eq. (26) adding the contributions of lines with $v^+ \leq 25$, $v'' \leq 10$, and $K^+, K'' \leq 12$. The adiabatic ionization energy of the $X^+\,^2B_1$ state of H_2O^+ was set to 12.621 eV, the value determined by Truong *et al.*[30] from the experimental TPES of water measured with synchrotron radiation between 12 and 40 eV photon energy. Assuming a temperature of 100 K and a Gaussian line shape with a half width at half maximum of 90 cm^{-1}, the TPES was computed and is plotted in Fig. 6. For emphasis purposes, three cases were treated. In the first and second ones, only $X^+\,^2B_1 \leftarrow X\,^1A_1$ and $A^+\,^2A_1 \leftarrow X\,^1A_1$ transitions were considered setting the $(q_v^-)^2$ and $(q_v^+)^2$ Franck-Condon factors to zero, respectively; in the third case all transitions were considered. The upper panel of Fig. 6 reveals that strong transitions spanning a small energy range arise near the ionization energy due to favorable Franck-Condon factors between the lower $X^+\,^2B_1$ RT substate and the ground $X\,^1A_1$ state. The spectrum in this upper panel resembles that shown in Fig. 3 of Truong *et al.*[30] except that the one calculated in this work does not display the Franck-Condon progression due to the stretching ν_1 mode. As emphasized by the middle panel, unfavorable Franck-Condon factors between the upper $A^+\,^2A_1$ RT substate and the ground $X\,^1A_1$ state lead to higher energy transitions. This calculated spectrum should be compared with Fig. 4 of Truong *et al.*[30] Even though, the ν_1 stretching mode is ignored, we can see that the Franck-Condon progression due to the ν_2 mode spans the same region than that in the observed spectrum. A comparison between the lower panel of Fig. 6 and the TPES in Fig. 2 of Truong *et al.*[30] reveals an agreement between the line intensities of the low and high energy portions of the spectrum.

The computed TPES could also be compared with the experimental photoelectron spectrum recorded by Ford *et al.*[31] using a higher resolution than Truong *et al.*[30] However such a comparison is outside the scope of the present paper as it requires a treatment of the photoionization cross section with values of l'' larger than one in Section IV.

B. CNC radical and CNC^+ ion

The rovibronic energy levels of the CNC radical in its ground $X\,^2\Pi_g$ electronic state were computed using the *ab initio* results in Section II and the procedure described in Section III B. Converged results were obtained setting $n_{\rm Max}$, P, and $\alpha, \alpha^{\pm}$ to 35, 38, and 20, respectively. For low lying rovibronic energy levels, Table III displays a comparison between

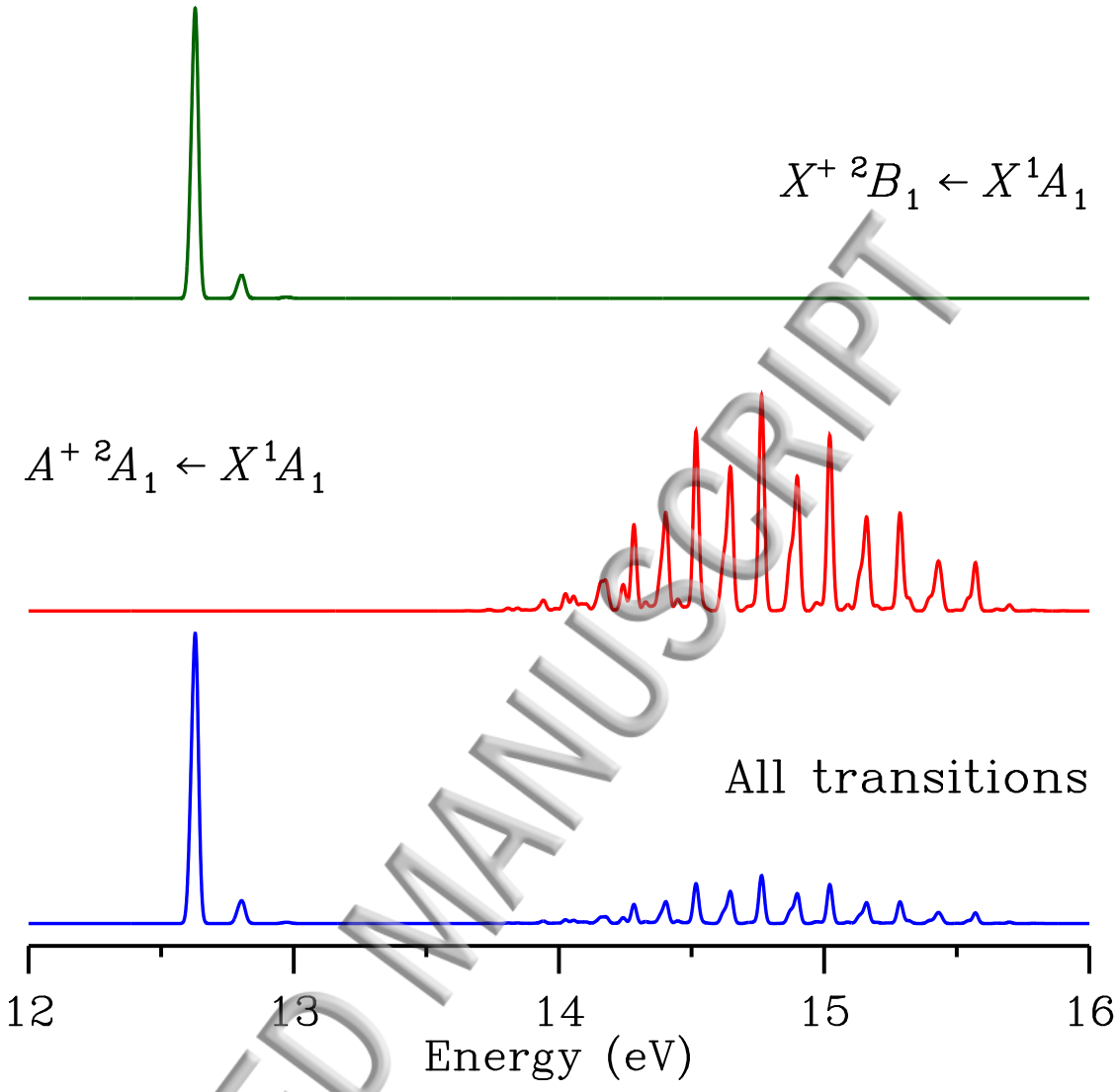

Figure 6. Simulated TPES of the $X^+\,^2\Pi_u \leftarrow X\,^1A_1$ ionizing transition of H_2O. In the upper and middle panel only $X^+\,^2B_1 \leftarrow X\,^1A_1$ and $A^+\,^2A_1 \leftarrow X\,^1A_1$ transitions were considered, respectively. All transitions are included in the lower panel.

the observed energies reported by Merer and Travis[34] and those calculated in this work. Observed minus calculated energies are within a few cm^{-1} except for the highest lying levels which is not involved in any of the vibronic transitions observed by Merer and Travis.[34]

The results of Sections II and III A were used to retrieve rovibrational energies for the CNC^+ cation. No experimental data are available for this species and energies could only be compared with those calculated by Jensen and Kraemer.[36] For the ν_2^0, $2\nu_2^0$, $3\nu_2^1$, and $4\nu_2^0$ states, the energies reported by these authors are 165, 349, 530, and 720 cm^{-1}, respectively,

Table III. Observed and calculated energies[a] for CNC

v_2	Γ	Obs.[b]	Cal.[c]
0	Π_g	−24	−24
1	Σ_u^-	120	117
1	Δ_u	248	245
2	Π_g	356	359
1	Σ_u^+	473	479
2	Φ_g	496	500
2	Π_g	855	802

[a] Rovibronic levels of the CNC radical are identified with the bent molecule vibrational quantum number v_2 and their symmetry species label Γ.

[b] Observed energy in cm^{-1} reported by Merer and Travis.[34]

[c] Energy in cm^{-1} calculated in Section V B taking the same energy origin as Merer and Travis.[34]

and are much larger than those calculated in this work: 96, 220, 350, and 494 cm^{-1}. The large differences stem from the fact that the bending potential retrieved in this work is much shallower and more anharmonic than that used by Jensen and Kraemer.[36]

The photoionization cross section were calculated with Eq. (26) for lines with $v^+ \leq 15$, $v'' \leq 30$, and $K^+, K'' \leq 21$. A Gaussian line shape with a half width at half maximum of 90 cm^{-1} was used when computing the photoelectron spectrum (PES). The energy difference between the cation and the neutral for the linear geometry, given in Section II, was shifted by +0.085 eV in order to obtain the best agreement between observed and calculated PES. This leads to an adiabatic ionization potential of 9.792 eV which is 0.012 eV larger than the value of Garcia *et al.*[6] Figure 7 shows experimental and calculated spectra. Unlike in H_2O, all transitions occur near the adiabatic ionization potential. This figure emphasizes that there is a small mismatch between the main peak maximum and the adiabatic ionization potential, which leads to the small discrepancy between the adiabatic ionization potential of this work and that of Garcia *et al.*[6] Almost no Franck-Condon progressions can be seen in the observed and calculated spectra because for all three electronic states the equilibrium configuration is the linear configuration. When using the bending potential of Jensen and Kraemer[36] for the cation, the agreement with the experimental spectrum is not as good

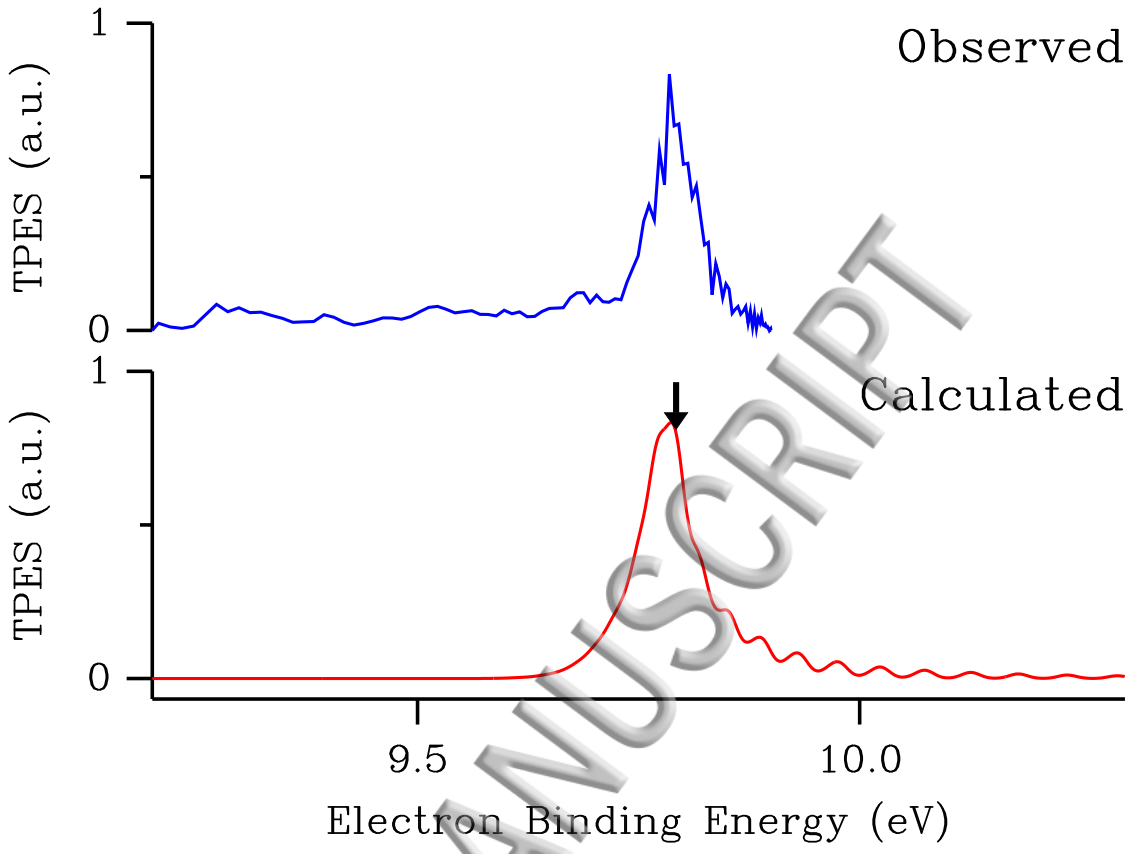

Figure 7. Observed[6] (Calculated) PES of the $X^+\,^1A_1 \leftarrow X\,^2\Pi_g$ ionizing transition of CNC in the upper (lower) panel. In the lower panel, the vertical arrow is the adiabatic ionization potential.

because the main peak in the calculated PES is narrower. A figure showing this calculated PES and the experimental one is available in the supplementary material.

C. CCN radical and CCN^+ ion

The rovibronic energy levels of the CCN radical and the CCN^+ cation were calculated as in the previous section. For the radical, Table IV lists the energies up to 1000 cm^{-1} along with those computed by Hill *et al.*[26] It can be seen that both sets of values are within 10 cm^{-1}. Merer and Travis[38] report for the energy difference of the $(010)\,^2\Delta$ and $(010)\,^2\Sigma^-$ levels a value of 113.55 cm^{-1} which compares well with that calculated in this work, 109 cm^{-1}. For the $(020)\,^2\Phi$ and $(010)\,^2\Sigma^-$ levels, the energies determined by Kohguchi *et al.*[41] with respect to the $(000)\,^2\Pi$ level are 573.84 and 179.27 cm^{-1} and also agree well with the present values: 574 and 183 cm^{-1}.

Table IV. Calculated rovibronic energies[a] for CCN

$(0v_20)$	Γ	Cal.[b]	Cal.[c]
(000)	Π	0	0
(010)	Σ^-	182	183
(010)	Δ	293	292
$(020)\mu$	Π	440	441
(010)	Σ^+	459	462
(020)	Φ	575	574
(030)	Σ^-	669	672
$(030)\mu$	Δ	713	715
$(020)\kappa$	Π	824	832
$(040)\mu$	Π	924	929
$(040)\mu$	Φ	993	996

[a] Levels are identified with the bent molecule vibrational quantum number v_2 and their symmetry species label Γ. Only levels below 1000 cm^{-1} appear.

[b] Calculated energy in cm^{-1} reported by Hill *et al.*[26] For doubly degenerate levels, the average value of the spin orbit components was taken.

[c] Energy in cm^{-1} calculated in Section V C.

For the CCN^+ cation, Jensen and Kraemer[36] determined the vibrational energies of the ν_2^1, $2\nu_2^0$, $3\nu_2^1$, and $4\nu_2^0$ states to be 153, 318, 482, and 650 cm^{-1}, respectively. These values are much larger than those obtained in this work: 104, 208, 318, and 430 cm^{-1}. Just as for CNC^+, this is due to the fact that the bending potential retrieved in this work is much shallower and more anharmonic than that used by Jensen and Kraemer.[36]

The photoionization cross sections were calculated as in the previous section and the TPES is shown in Fig. 8. The energy difference between the cation and the neutral for the linear geometry, given in Section II, was shifted by +0.080 eV in order to obtain the best agreement between observed and calculated TPES. This leads to an adiabatic ionization potential of 10.822 eV, which agrees well with the value of Garcia *et al.*[6] Most transitions are located near this energy. For the calculated spectrum, a Franck-Condon progression can clearly be seen on the high energy side of the main peak and a matching weak feature can be

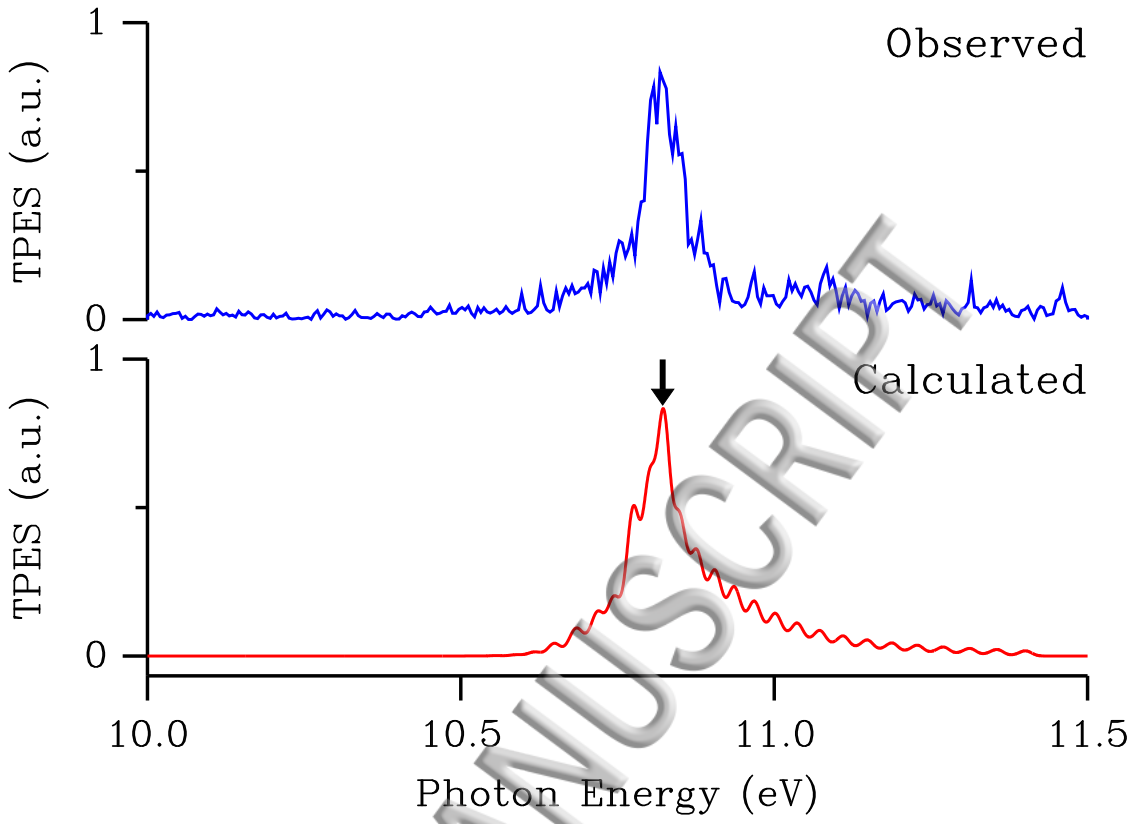

Figure 8. Observed[6] (Calculated) TPES of the $X^+\,^1A' \leftarrow X\,^2\Pi$ ionizing transition of CCN in the upper (lower) panel. In the lower panel, the vertical arrow is the adiabatic ionization potential.

observed in the experimental spectrum. Lowering the temperature leads to a narrower main peak but does not really improve the agreement between observed and calculated spectra on the high energy side of the main peak.

D. HCCN radical and $HCCN^+$ ion

Setting $n_{\rm Max}$, P, and $\alpha, \alpha^{\pm}$ to 40, 43, and 20, respectively, rovibronic energies were obtained for HCCN and $HCCN^+$. For the former species, vibrational states are labeled using the linear molecule quantum numbers ${v_5}^{l_5}$ and their energies are given up to $v_5 = 4$ in Table V. These values should be compared with those in Tables 6 and 9 of Koput.[32] Experimental energies of 128.9, 341.7, and 625 cm^{-1} are available for the 1^1, 2^2, and 3^3 states, respectively, and are in better agreement with the present calculated energies than with those calculated by Koput.[32] The vibronic energies calculated for the cation are consistent with a large RT interaction. To our knowledge no spectroscopic investigation of the cation is

Table V. Calculated vibrational energies[a] for HCCN

$v_5{}^{l_5}$	E^{b}	$v_5{}^{l_5}$	E^{b}	$v_5{}^{l_5}$	E^{b}
0^0	0	2^0	459	4^4	921
1^1	125	3^3	603	4^2	1015
2^2	334	3^1	719	4^0	1066

[a] Levels are identified using the linear molecule vibrational quantum numbers $v_5{}^{l_5}$.
[b] Energies in cm^{-1} calculated in Section V D.

available in the literature.

The photoionization cross section was calculated with Eq. (26) for lines with $v^+ \leq 40$, $v'' \leq 20$, and $K^+, K'' \leq 30$. A Gaussian line shape with a half width at half maximum of 90 cm^{-1} was taken when computing the TPES, plotted in Fig. 9. About half of the transitions are located near 10.65 eV. The other half are spread over the region from 10.8 to 11.5 eV corresponding to a superposition of many Franck-Condon progressions. Unlike in CNC and CCN, the bending potential of the ground $X\,^3A''$ state is quite different from those of the two upper electronic states, leading to a large number of such progressions. The energy difference between the cation and the neutral for the linear geometry, given in Section II, was decreased by 0.010 eV so as to obtain the best agreement between observed and calculated TPES. The value calculated for the adiabatic ionization potential is then 10.621 eV. This value is 0.118 eV above that reported by Zhao *et al.*[39] and 0.021 eV below that obtained by Garcia *et al.*[6] This discrepancy, larger than in the case of CNC, is also due to the fact that the adiabatic ionization potential differs from the experimental energy of the main peak maximum, as emphasized by Figure 9. This latter value was incorrectly taken as the adiabatic ionization potential in Garcia *et al.*[6]

VI. DISCUSSION

Calculated photoelectron spectra are computed for the CNC, CCN, and HCCN radicals based on a derived expression of the total photoionization cross section when one of the electronic states is affected by the RT effects. Two approaches aimed at spectroscopically modeling the quasilinearity and the RT coupling displayed by these species are also derived.

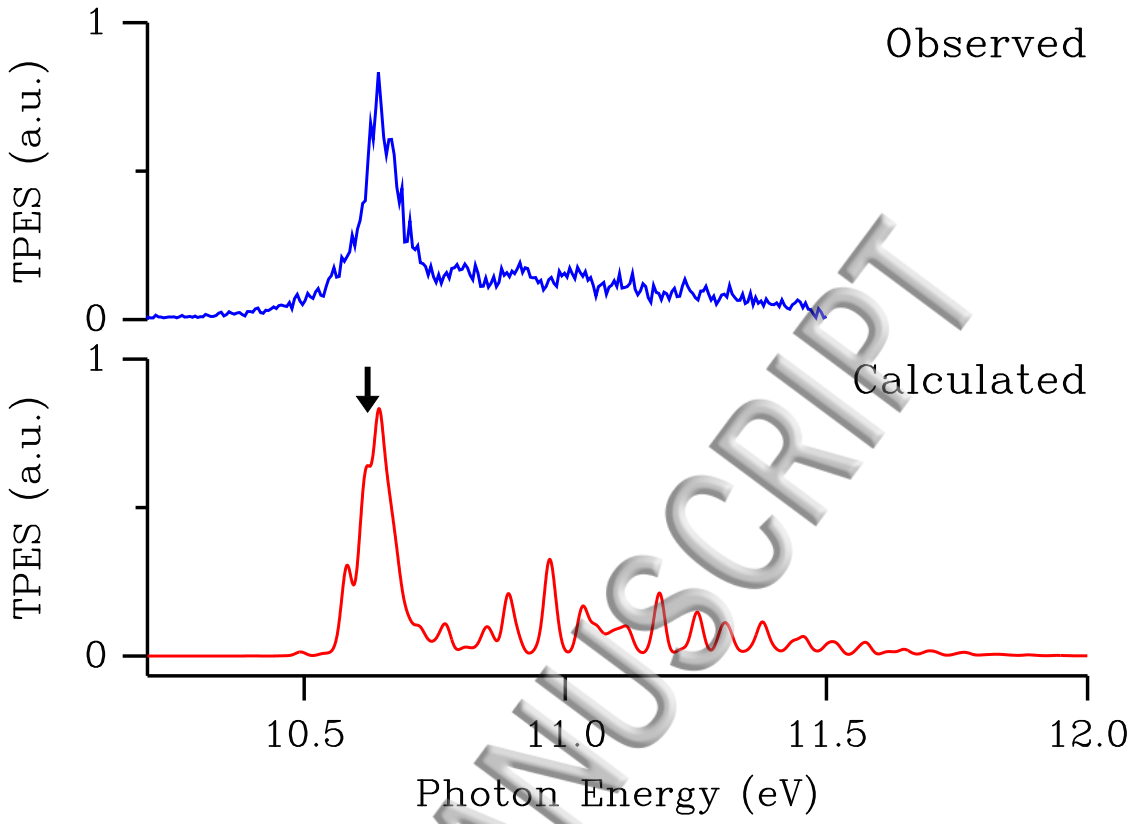

Figure 9. Observed[6] (Calculated) TPES of the $X^+\,^2\Pi \leftarrow X\,^3A''$ ionizing transition of HCCN in the upper (lower) panel. In the lower panel, the small vertical arrow is the adiabatic ionization potential.

The total photoionization cross section obtained in this work, appearing in Eq. (21), was derived making use of the results of Willitsch *et al.*[15] for the total photoionization cross section of an asymmetric top molecule. Their expression, obtained using the orbital approximation, is conveniently expanded in terms of products of rotational, vibrational, and electronic terms. In this work, the RT coupling taking place in one of the electronic states is dealt with by adding the contribution of both RT components of the ionizing electronic transition. The vibrational term is written in terms of Franck-Condon factors involving the bending wavefunctions.

In the approaches accounting for the quasilinearity and the RT coupling, introduced in Section III, the overall rotation and the bending mode are treated together, accounting for the large amplitude nature of this mode. These approaches allow us to describe well the bending-rotation and the rovibronic couplings, but they only provide us with a limited

description as they ignore the electron spin and the stretching modes. This approximate description should nonetheless be sufficient for the qualitative results sought in this paper. A more satisfactory description would be achieved with treatments accounting for all vibrational modes.[27,51,52]

In order to understand qualitatively the contribution of the various terms in the new expression of the total photoionization cross section, the theoretical treatment was first applied, in Section V A, to the simulation of the photoelectron spectrum of H_2O for which both the neutral[28] and the cationic[29] species are spectroscopically well characterized; the latter displaying a strong RT coupling with a Renner parameter larger than 1. The calculated TPES, displayed in Fig. 6, is in qualitative agreement with the experimental one.[30]

The theoretical approach was then applied to the computation of the photoelectron spectra of CNC, CCN, and HCCN. The bending potentials of these species were retrieved using the *ab initio* calculations presented in Section II and their rovibronic energies, computed in Sections V B, V C and V D, turned out to be in good agreement with spectroscopic data[34,38,41] and calculations.[26,32] Adjusting the adiabatic ionization potential of each molecule, a qualitative agreement between their experimental[6] and calculated PES or TPES was achieved and can be seen in Figs. 7–9. For CNC, both spectra display a single peak. Matching the energy of these peaks, the adiabatic ionization potential, deduced from Section V B, was increased by 0.085 eV and was found to be 9.792 eV. For CCN, both spectra span a larger energy range and the improved value of the vertical ionization potential, 0.080 eV higher than the value from Section V C, is 10.822 eV. For HCCN, both spectra display a narrow peak and a broad feature. Matching these spectra leads to an adiabatic ionization potential of 10.621 eV, which is 0.010 eV smaller than the value calculated in Section V D.

Appendix A: Matrix elements of inverse inertia tensor components

The matrix element of the diagonal component $\mu_{zz}(t)$ of the inverse inertia tensor between two basis set functions of Eq. (4) is equal to:

$$\langle \theta_n^{\alpha\beta} | \mu_{zz}(t) | \theta_m^{\alpha\beta} \rangle = \int_{-1}^{+1} dt\, \mu_{zz}(t)\, (1-t)^{\alpha} \times (1+t)^{\beta}\, P_n^{(\alpha,\beta)}(t)\, P_m^{(\alpha,\beta)}(t) / \sqrt{h_n h_m}. \tag{A1}$$

The matrix element of the kinetic energy operator $P_t\mu_{tt}(t)P_t$ can be obtained from:

$$\langle\theta_n^{\alpha\beta}|P_t\mu_{tt}(t)P_t|\theta_m^{\alpha\beta}\rangle = \int_{-1}^{+1} dt\,\mu_{tt}(t)\,(1-t)^{\alpha-2} \times (1+t)^{\beta-2}\,D_n^{(\alpha,\beta)}(t)\,D_m^{(\alpha,\beta)}(t)/\sqrt{h_n h_m}, \tag{A2}$$

where, in agreement with Partridge and Schwenke,[28] $D_n^{(\alpha,\beta)}(t)$ is a polynomial expressed in terms of the Jacobi polynomial $P_n^{(\alpha,\beta)}(t)$ and its derivative $P_n^{(\alpha,\beta)\prime}(t)$ as:

$$D_n^{(\alpha,\beta)}(t) = P_n^{(\alpha,\beta)}(t)[(\alpha-\beta)/2 + t(\alpha+\beta)/2] - (1-t^2)P_n^{(\alpha,\beta)\prime}(t). \tag{A3}$$

Evaluating the matrix elements in Eqs. (A1) and (A2) with a P-point Gauss-Jacobi quadrature suited for the weight function $(1-t)^{\alpha-1}(1+t)^{\beta-1}$, the quadrature leads to:

$$\langle\theta_n^{\alpha\beta}|\mathrm{Op}|\theta_m^{\alpha\beta}\rangle = \sum_{i=1}^{P}\omega_i f(t_i), \tag{A4}$$

where ω_i and t_i are respectively the weights and nodes. When $\mathrm{Op} = \mu_{zz}(t)$, the function $f(t)$ is:

$$f(t) = P_n^{(\alpha,\beta)}(t)\,P_m^{(\alpha,\beta)}(t)\,(1-t^2)\,\mu_{zz}(t)/\sqrt{h_n h_m}. \tag{A5}$$

When $\mathrm{Op} = P_t\mu_{tt}(t)P_t$, the function $f(t)$ is:

$$f(t) = D_n^{(\alpha,\beta)}(t)\,D_m^{(\alpha,\beta)}(t)\frac{\mu_{tt}(t)}{(1-t^2)}/\sqrt{h_n h_m}. \tag{A6}$$

Equations (3) and (A3) show that in both cases $f(t)$ is a finite smooth function of t and the quadrature should lead to accurate results.

SUPPLEMENTARY MATERIAL

See supplementary material for a PDF file containing four figures numbered S1 to S4. Figures S1–S3 illustrate the fit of the bond lengths. Figure S4 shows a comparison between observed and calculated PES for CNC.

REFERENCES

[1]S. Willitsch, U. Hollenstein, and F. Merkt, J. Chem. Phys. **120**, 1761 (2004).

[2]R. Signorell and F. Merkt, Faraday Discuss. **115**, 205 (2000).

[3]S. T. Pratt, P. M. Dehmer, and J. L. Dehmer, J. Chem. Phys. **95**, 6238 (1991).

[4]S. T. Pratt, P. M. Dehmer, and J. L. Dehmer, J. Chem. Phys. **99**, 6233 (1993).

[5]A. N. Petelin and A. A. Kiselev, Int. J. Quantum Chem. **6**, 701 (1972).

[6]G. A. Garcia, J. Krüger, B. Gans, C. Falvo, L. H. Coudert, and J.-C. Loison, J. Chem. Phys. **147**, 013908 (2017).

[7]A. D. Buckingham, B. J. Orr, and J. M. Sichel, Philos. Trans. R. Soc. London, Ser. A **268**, 147 (1970).

[8]J. Xie and R. N. Zare, J. Chem. Phys. **93**, 3033 (1990).

[9]J. Xie and R. N. Zare, J. Chem. Phys. **97**, 2891 (1992).

[10]F. Merkt and T. P. Softley, Int. Rev. Phys. Chem. **12**, 205 (1993).

[11]M. S. Child and C. Jungen, J. Chem. Phys. **93**, 7756 (1990).

[12]K. Müller-Dethlefs, J. Chem. Phys. **95**, 4821 (1991).

[13]R. Signorell and F. Merkt, Mol. Phys. **92**, 793 (1997).

[14]S. Willitsch, J. M. Dyke, and F. Merkt, Mol. Phys. **102**, 1543 (2004).

[15]S. Willitsch and F. Merkt, Int. J. Mass Spec. **245**, 14 (2005).

[16]L. H. Coudert, J. Mol. Spectrosc. **154**, 427 (1992).

[17]L. H. Coudert, J. Mol. Spectrosc. **165**, 406 (1994).

[18]L. H. Coudert, J. Mol. Spectrosc. **181**, 246 (1997).

[19]R. Lanquetin, L. H. Coudert, and C. Camy-Peyret, J. Mol. Spectrosc. **195**, 54 (1999).

[20]L. H. Coudert, Mol. Phys. **96**, 941 (1999).

[21]L. H. Coudert, J. Mol. Spectrosc. **330**, 112 (2016).

[22]C. Jungen and A. J. Merer, Mol. Phys. **40**, 1 (1980).

[23]S. Carter and N. C. Handy, Mol. Phys. **52**, 1367 (1984).

[24]M. Perić, S. D. Peyerimhoff, and R. J. Buenker, Int. Rev. Phys. Chem. **4**, 85 (1985).

[25]A. Alijah and G. Duxbury, J. Mol. Spectrosc. **211**, 7 (2002).

[26]J. G. Hill, A. Mitrushchenkov, K. E. Yousaf, and K. A. Peterson, J. Chem. Phys. **135**, 144309 (2011).

[27]A. O. Mitrushchenkov, J. Chem. Phys. **136**, 024108 (2012).

[28]H. Partridge and D. W. Schwenke, J. Chem. Phys. **106**, 4618 (1997).

[29]S. Wu, Y. Chen, X. Yang, Y. Guo, Y. Liu, Y. Li, R. J. Buenker, and P. Jensen, J. Mol. Spectrosc. **225**, 96 (2004).

[30]G. Y. Truong, A. J. Yencha, A. M. Juarez, S. J. Cavanagh, P. Bolognesi, and G. C. King, Chem. Phys. **355**, 183 (2009).

[31]M. S. Ford, K. Müller-Dethlefs, M. Kitajima, H. Tanaka, Y. Tamenori, A. De Fanis, and K. Ueda, J. Phys. Chem. A **114**, 11133 (2010).

[32]J. Koput, J. Phys. Chem. A **106**, 6183 (2002).

[33]F. Brown, S. Saito, and S. Yamamoto, J. Mol. Spectrosc. **143**, 203 (1990).

[34]A. J. Merer and D. N. Travis, Can. J. Phys. **44**, 353 (1966).

[35]Rajendra Pd. and P. Chandra, J. Chem. Phys. **114**, 1589 (2001).

[36]P. Jensen and W. P. Kraemer, J. Mol. Spectrosc. **129**, 216 (1988).

[37]M. Wyss, E. Riaplov, J. P. Maier, M. Hochlaf, and P. Rosmus, Helv. Chim. Acta **84**, 1432 (2001).

[38]A. J. Merer and D. N. Travis, Can. J. Phys. **43**, 1795 (1965).

[39]Z.-X. Zhao, H.-X. Zhang, and C.-C. Sun, J. Phys. Chem. A **112**, 12125 (2008).

[40]N. Inostroza, X. Huang, and T. J. Lee, J. Chem. Phys. **135**, 244310 (2011).

[41]H. Kohguchi, Y. Ohshima, and Y. Endo, J. Chem. Phys. **106**, 5429 (1997).

[42]M. C. McCarthy, C. A. Gottlieb, A. L. Cooksy, and P. Thaddeus, J. Chem. Phys. **103**, 7779 (1995).

[43]C. Camy-Peyret and J.-M. Flaud, Mol. Phys. **32**, 523 (1976).

[44]J. T. Hougen, P. R. Bunker, and J. W. C. Johns, J. Mol. Spectrosc. **34**, 136 (1970).

[45]M. A. Mekhtiev, P. D. Godfrey, and V. Szalay, J. Mol. Spectrosc. **180**, 42 (1996).

[46]M. Abramowitz and I. A. Stegun, *Handbook of mathematical functions with formulas, graphs, and mathematical tables*, National Bureau of Standards Applied Mathematics Series, Vol. 55 (For sale by the Superintendent of Documents, U.S. Government Printing Office, Washington, D.C., 1964) pp. xiv+1046.

[47]E. P. Wigner, *Group Theory* (Academic Press, New York, 1959).

[48]P. R. Bunker, *Molecular Symmetry and Spectroscopy*, 1st ed. (Academic Press, New York, 1979).

[49]C. Jungen, K.-E. J.Hallin, and A. J. Merer, Mol. Phys. **40**, 25 (1980).

[50]P. R. Bunker and J. M. R. Stone, J. Mol. Spectrosc. **41**, 310 (1972).

[51]G. Duxbury, B. D. McDonald, M. V. Gogh, A. Alijah, C. Jungen, and H. Palivan, J. Chem. Phys. **108**, 2336 (1998).

[52] P. Jensen, T. E. Odaka, W. P. Kraemer, T. Hirano, and P. R. Bunker, Spectrochim. Acta. A **58**, 763 (2002).

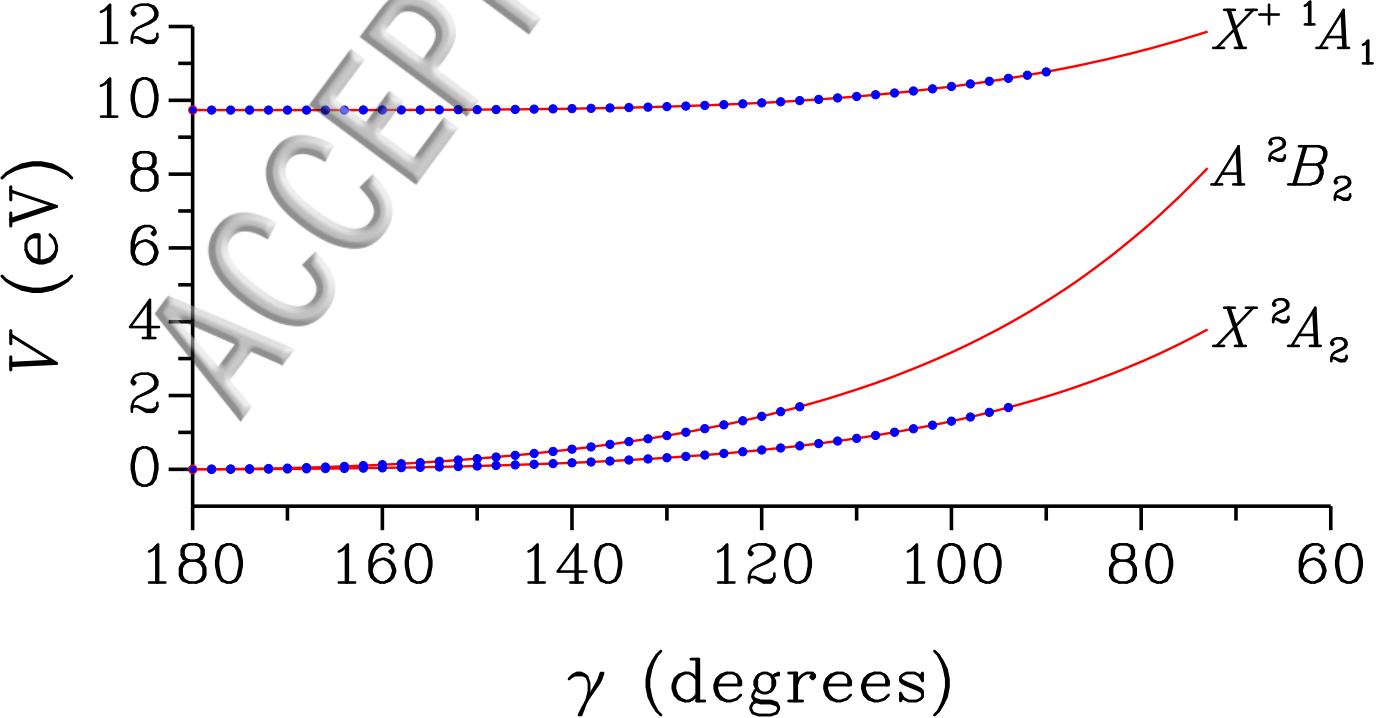
12
10
8
6
4
2
0
V (eV)
180
160
140
120
100
80
60
γ (degrees)
X+ 1A1
A 2B2
X 2A2

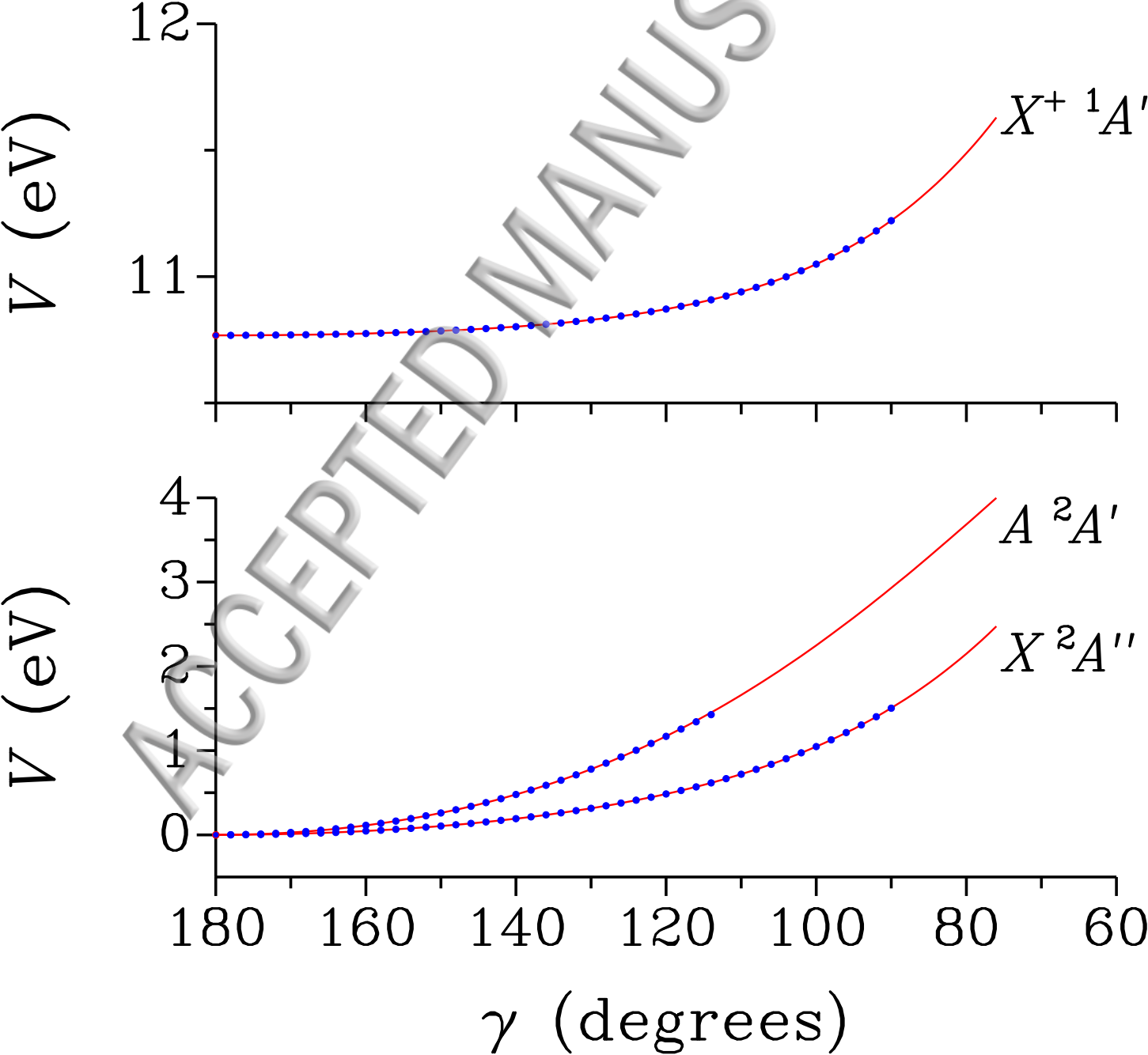

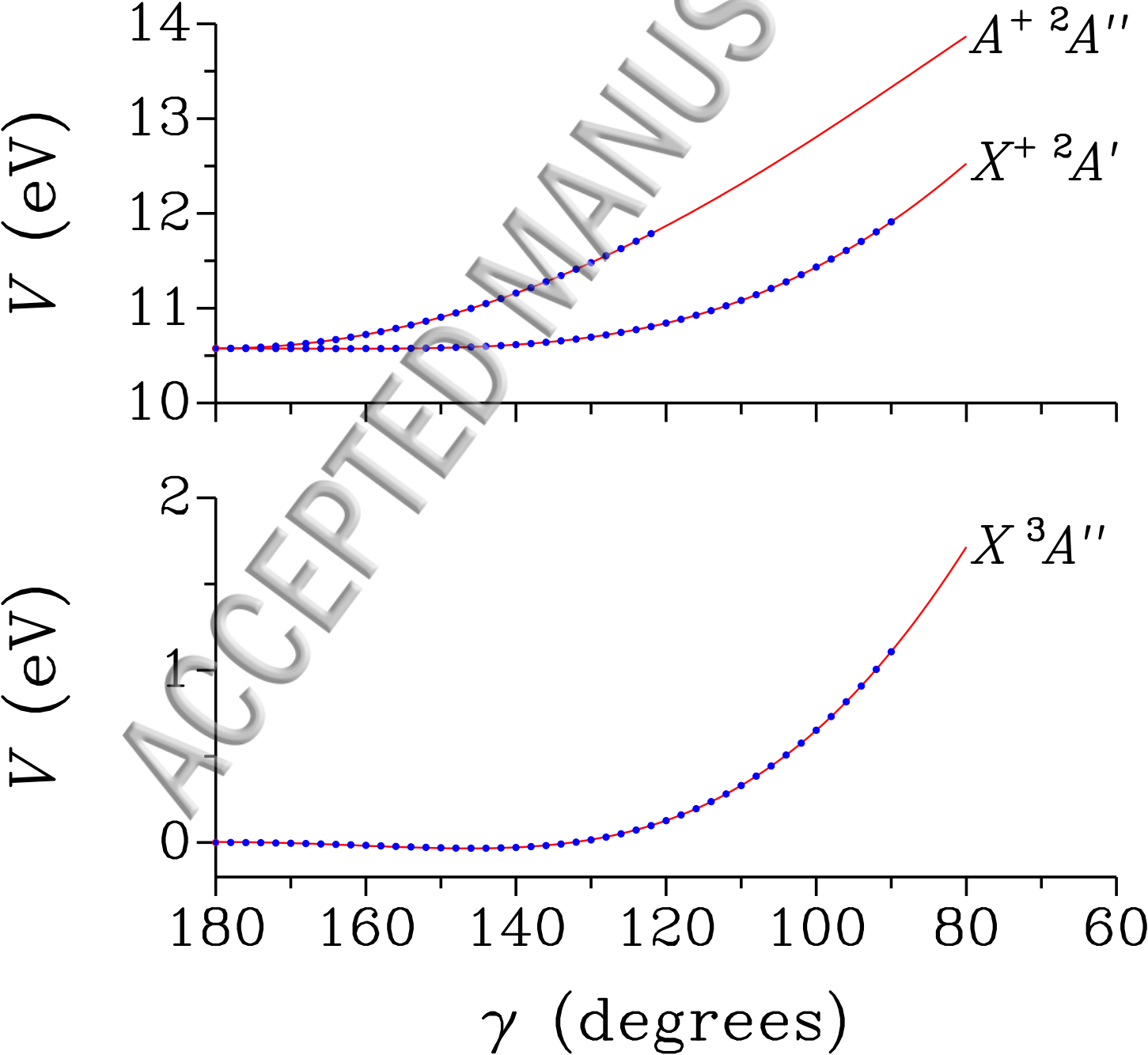

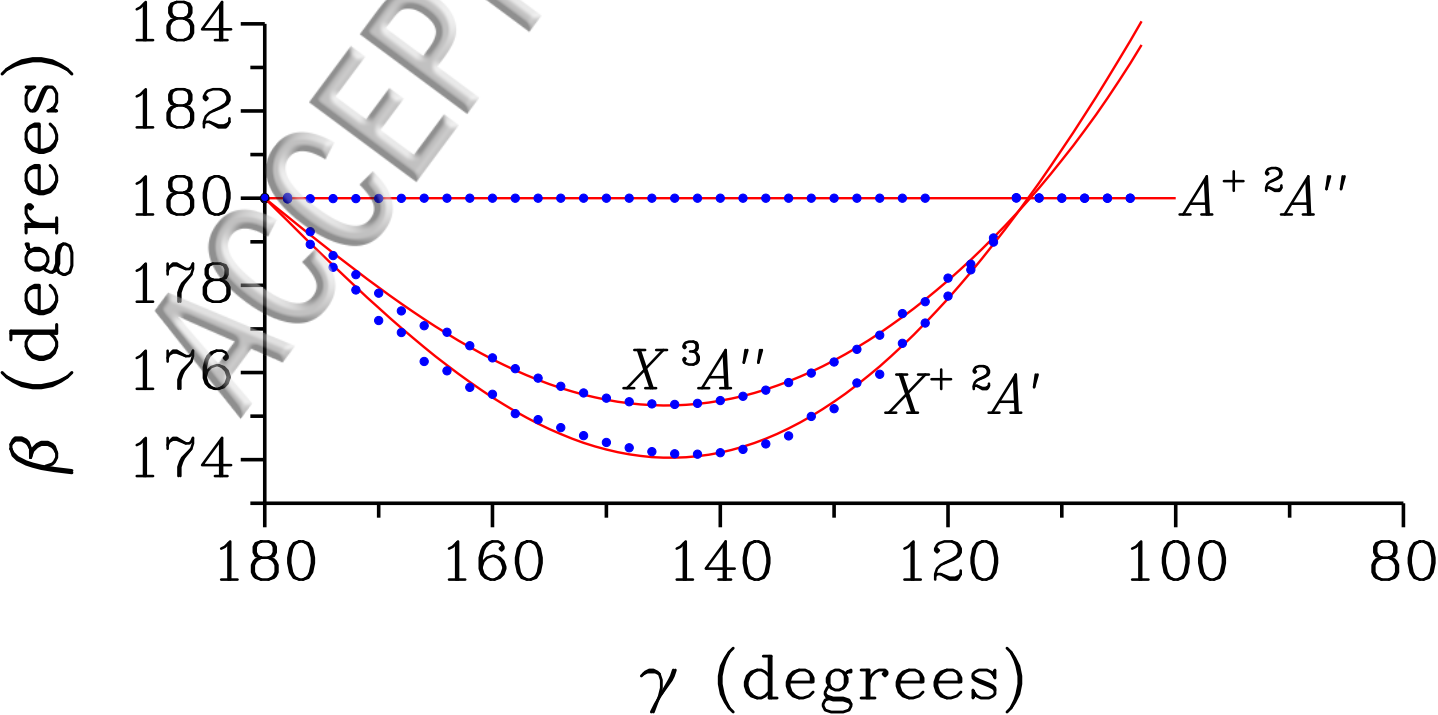
184
182
180
178
176
174
β (degrees)
180
160
140
120
100
80
γ (degrees)
A+ 2A''
X 3A''
X+ 2A'

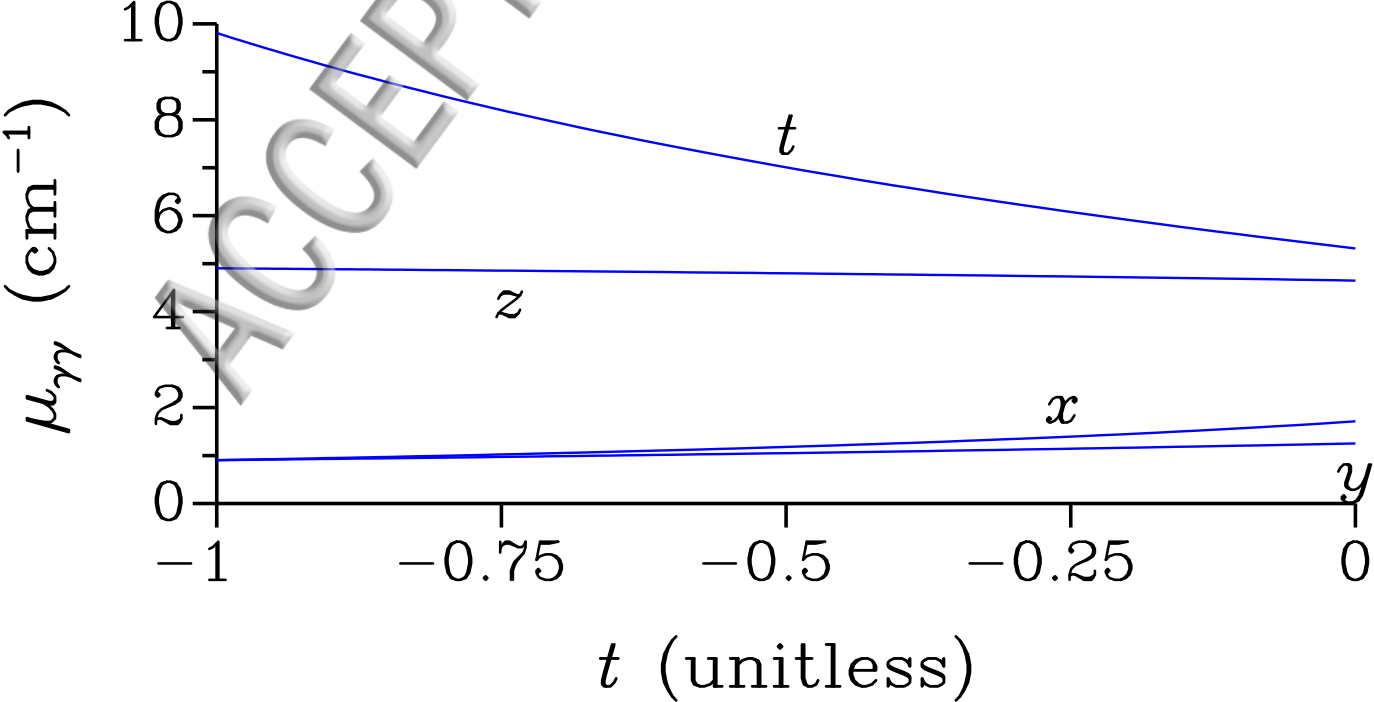

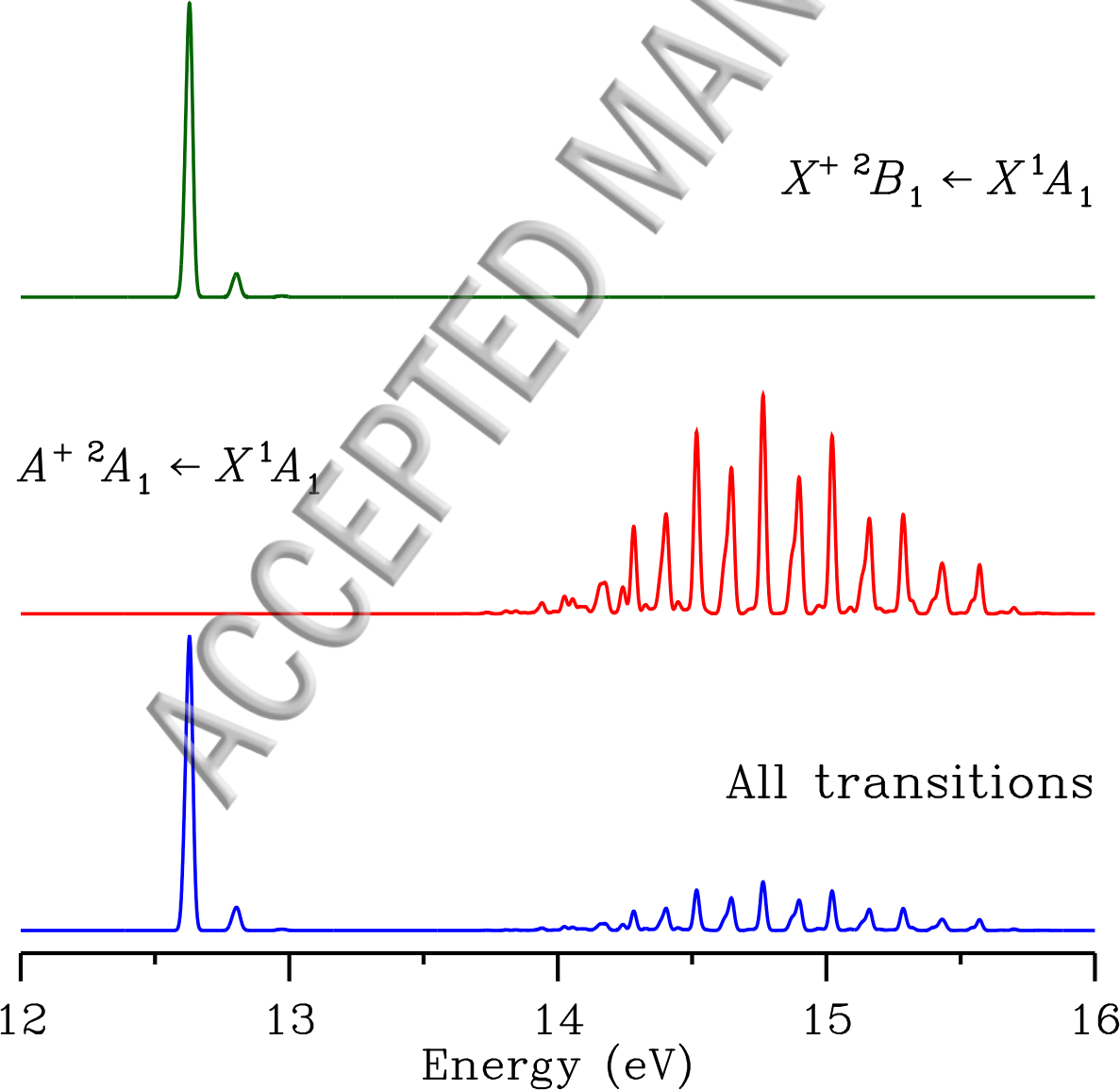

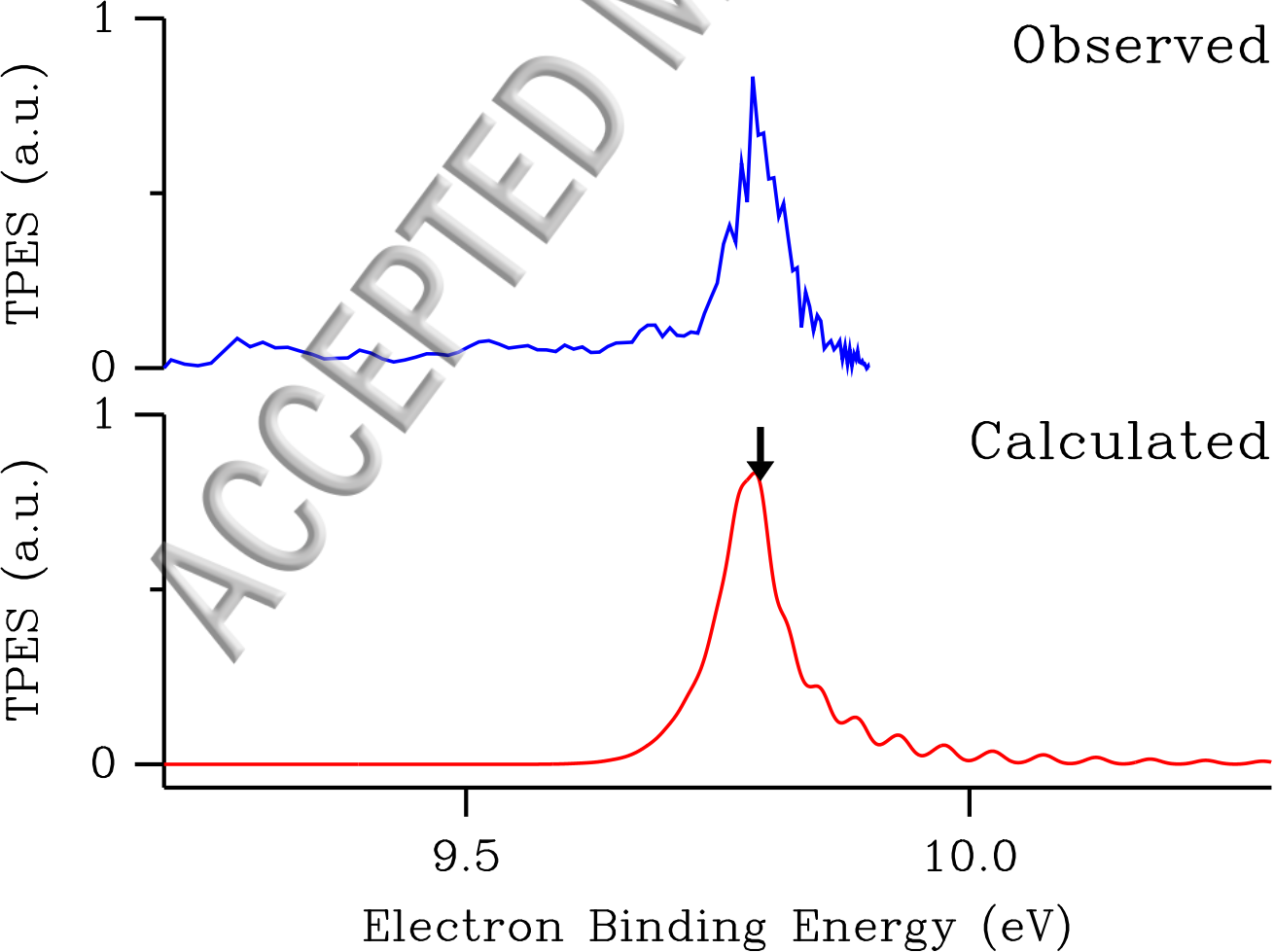
Observed
Calculated
TPES (a.u.)
TPES (a.u.)
1
0
1
0
9.5
10.0
Electron Binding Energy (eV)

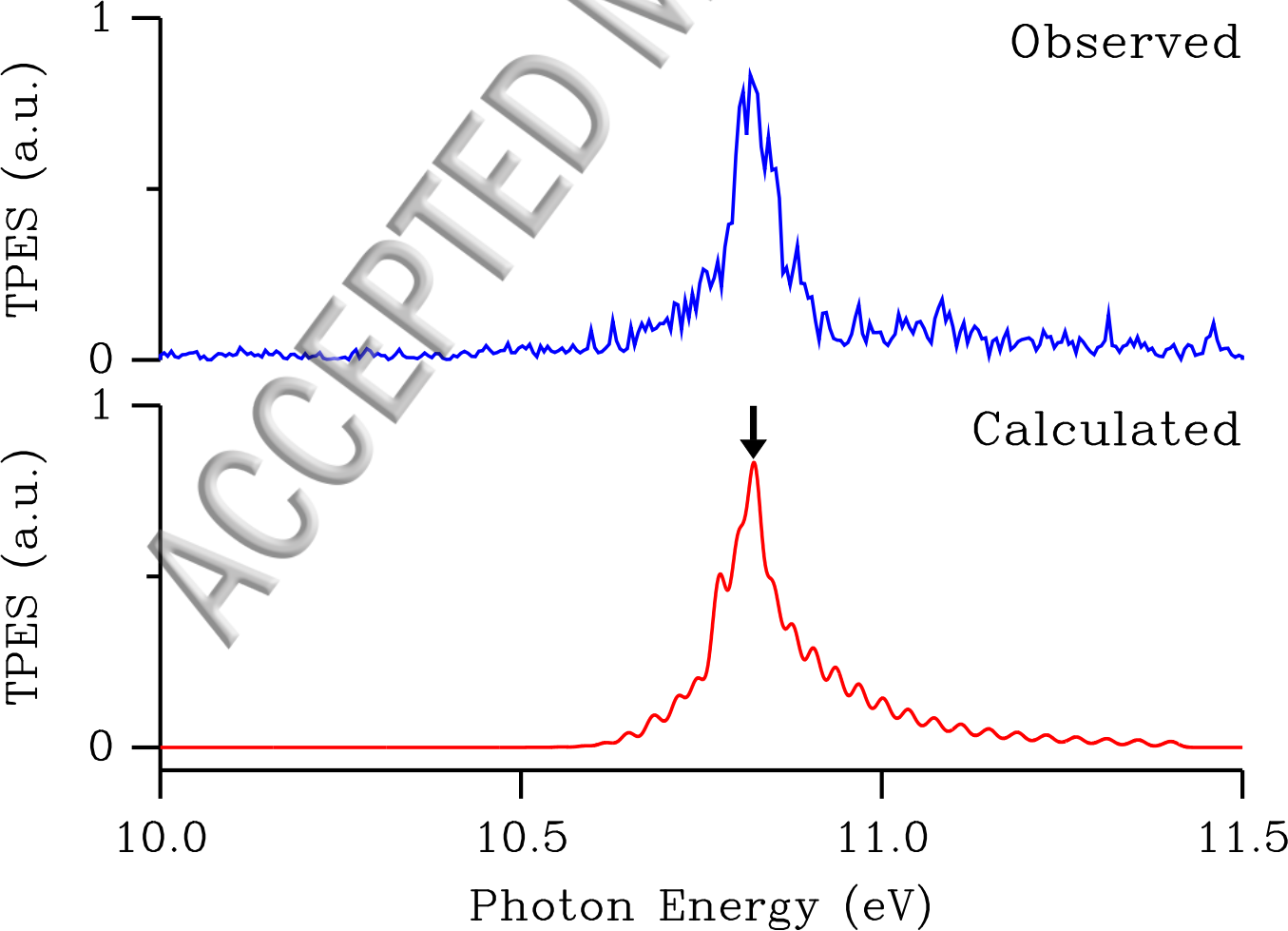
Observed
Calculated
TPES (a.u.)
TPES (a.u.)
1
0
1
0
10.0
10.5
11.0
11.5
Photon Energy (eV)

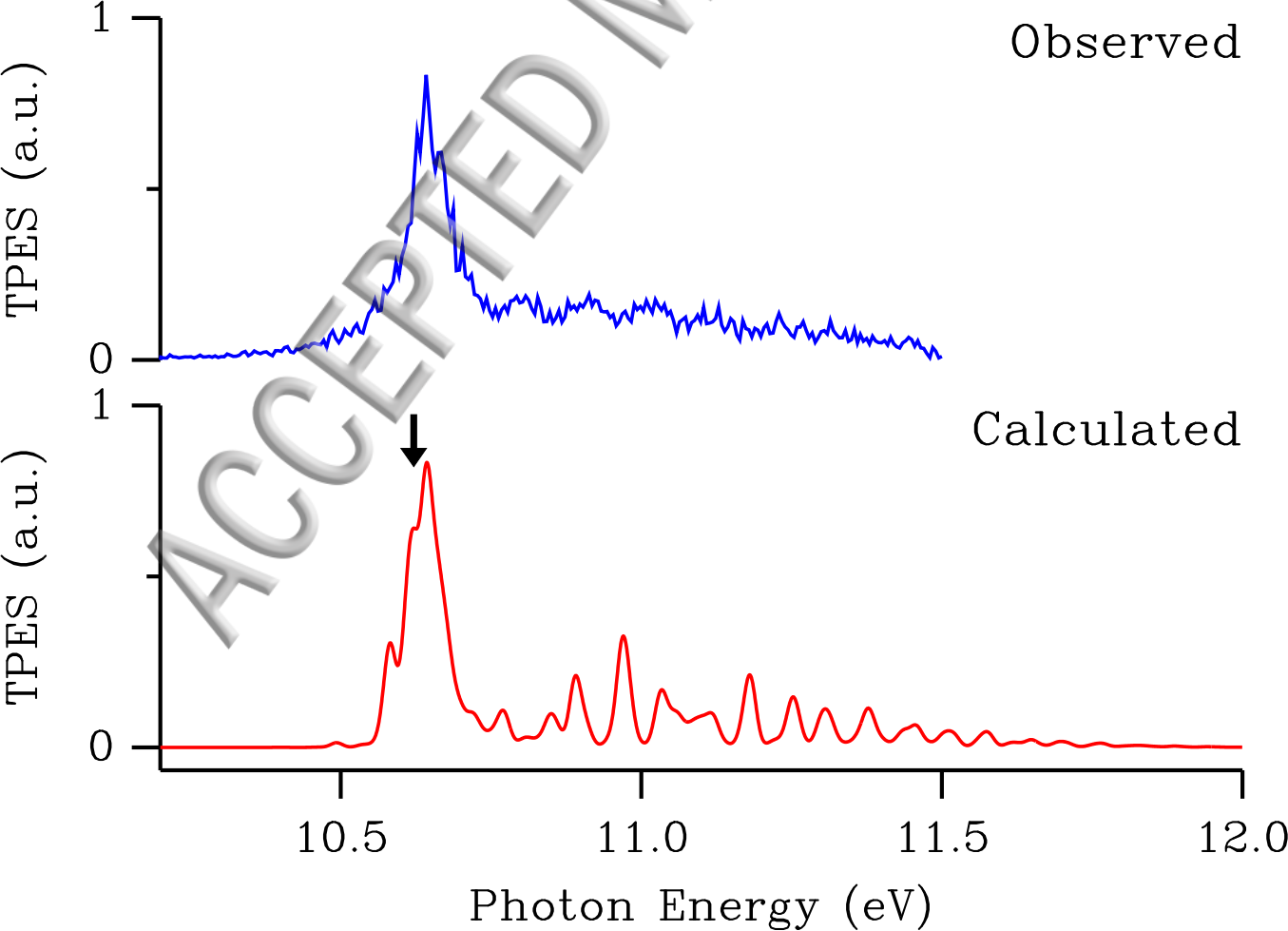
Observed
Calculated
TPES (a.u.)
TPES (a.u.)
1
0
1
0
10.5
11.0
11.5
12.0
Photon Energy (eV)